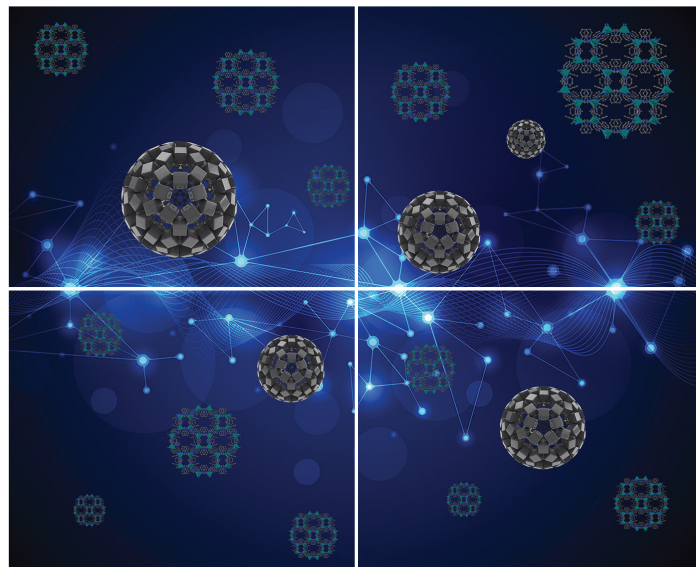


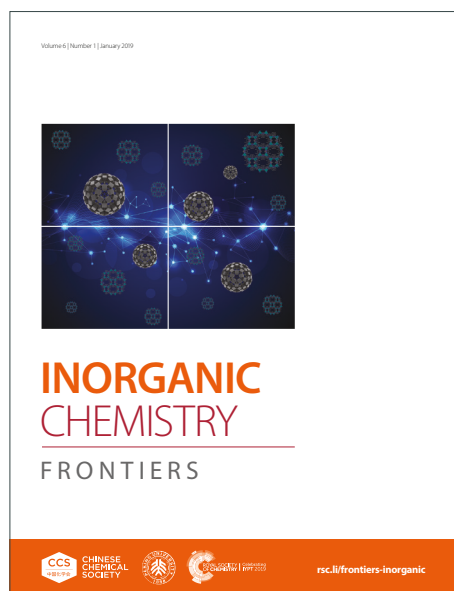
# INORGANIC CHEMISTRY

## FRONTIERS

Accepted Manuscript



This article can be cited before page numbers have been issued, to do this please use: M. Tosato, F. Ponte, S. Franchi, N. May, M. Jensen, H. Maecke, V. Di Marco, L. Pigani, E. Ferrari, E. Sicilia, M. Asti and C. F. Ramogida, *Inorg. Chem. Front.*, 2026, DOI: 10.1039/D6QI00525J.



This is an Accepted Manuscript, which has been through the Royal Society of Chemistry peer review process and has been accepted for publication.

Accepted Manuscripts are published online shortly after acceptance, before technical editing, formatting and proof reading. Using this free service, authors can make their results available to the community, in citable form, before we publish the edited article. We will replace this Accepted Manuscript with the edited and formatted Advance Article as soon as it is available.

You can find more information about Accepted Manuscripts in the [Information for Authors](#).

Please note that technical editing may introduce minor changes to the text and/or graphics, which may alter content. The journal's standard [Terms & Conditions](#) and the [Ethical guidelines](#) still apply. In no event shall the Royal Society of Chemistry be held responsible for any errors or omissions in this Accepted Manuscript or any consequences arising from the use of any information it contains.

# A Hybrid Pyridine-Thioether Macrocycle to Chelate Theranostic Copper and Silver Radioisotopes

Marianna Tosato<sup>1,2,\*</sup>, Fortuna Ponte<sup>3</sup>, Sara Franchi<sup>4</sup>, Nora V. May<sup>5</sup>, Mikael Jensen<sup>6</sup>, Helmut Mäcke<sup>7</sup>, Valerio Di Marco<sup>4</sup>, Laura Pigani<sup>8</sup>, Erika Ferrari<sup>8</sup>, Emilia Sicilia<sup>3</sup>, Mattia Asti<sup>9</sup> and Caterina F. Ramogida<sup>1,2,\*</sup>

<sup>1</sup> Department of Chemistry, Simon Fraser University, V5A 4Y8 Burnaby, British Columbia, Canada

<sup>2</sup> Life Sciences, TRIUMF, V6T 2A3 Vancouver, British Columbia, Canada

<sup>3</sup> Department of Chemistry and Chemical Technologies, University of Calabria, 87036 Cosenza, Italy

<sup>4</sup> Department of Chemical Sciences, University of Padova, 35131 Padova, Italy

<sup>5</sup> Centre for Structural Science, Research Centre for Natural Sciences, 1117 Budapest, Hungary

<sup>6</sup> The Hevesy Laboratory, Department of Health Technology, Technical University of Denmark, 4000 Roskilde, Denmark

<sup>7</sup> Department of Nuclear Medicine, University Hospital Freiburg, D-79106 Freiburg, Germany

<sup>8</sup> Department of Chemical and Geological Sciences, University of Modena and Reggio Emilia, 41125 Modena, Italy

<sup>9</sup> Radiopharmaceutical Chemistry Laboratory, Nuclear Medicine Unit, AUSL-IRCCS Reggio Emilia, 42122 Reggio Emilia, Italy

**Corresponding authors:** [marianna\\_tosato@sfu.ca](mailto:marianna_tosato@sfu.ca); [cfr@sfu.ca](mailto:cfr@sfu.ca)

## Abstract

Coinage radiometals such as <sup>64/67</sup>Cu and <sup>103/111</sup>Ag offer unique opportunities for cancer theranostics, providing matched diagnostic and therapeutic radionuclides within the same chemical family. However, their clinical translation is limited by the lack of robust chelators for <sup>103/111</sup>Ag and by the redox-induced instability of <sup>64/67</sup>Cu complexes. To address these chelation challenges, we developed DO2S2Py, a sulfur-containing cyclen (cy)-based macrocycle incorporating pyridine (py) donors, introduced to create a protected coordination environment for silver and copper ions.

DO2S2Py rapidly forms highly thermodynamically stable and kinetically inert 1:1 metal-to-ligand complexes with both Cu<sup>2+</sup> and Ag<sup>+</sup>. Structural investigations reveal distinct yet strongly stabilized coordination environments for Cu<sup>2+</sup> (4N<sub>cy</sub>2N<sub>py</sub>) and Ag<sup>+</sup> (4N<sub>cy</sub>1N<sub>py</sub>1S and 4N<sub>cy</sub>2N<sub>py</sub>), underscoring the crucial contribution of the pyridine donors. Under highly diluted radiochemical conditions and mild labeling protocols, DO2S2Py efficiently binds <sup>64</sup>Cu and <sup>111</sup>Ag. The <sup>64</sup>Cu complex demonstrates exceptional stability in PBS and human serum (> 95% intact complex after 24 h), while the <sup>111</sup>Ag analogue, though somewhat less stable (75% intact after 24 h), outperforms the current gold-standard chelator. These findings validate the incorporation of pyridine donors as an effective strategy toward unified chelation of theranostic coinage radiometals.

**Keywords:** Cancer, Theranostic, Coordination Chemistry, Radiometals



## 1. Introduction

The integration of radiometals into diagnostic and therapeutic radiopharmaceuticals has significantly advanced the field of precision medicine, enabling cancer imaging and targeted therapy at the molecular level. Within the broad spectrum of medically relevant radionuclides, group 11 radiometals, particularly copper and silver radioisotopes, have emerged as attractive candidates due to their favorable decay characteristics and suitability for diagnostic and therapeutic (*theranostic*) approaches.<sup>1–4</sup>

Among these, copper-64 (<sup>64</sup>Cu,  $t_{1/2}$  = 12.7 h) has a versatile emission profile that includes  $\beta^-$ ,  $\beta^+$  and electron capture decays and is highly suited for positron emission tomography (PET).<sup>5</sup> Complementarily, copper-67 (<sup>67</sup>Cu,  $t_{1/2}$  = 2.58 d) is a pure  $\beta^-$  emitter with accompanying low energy conversion and Auger electrons as well as  $\gamma$  rays that make it a candidate for therapy and single photon emission computed tomography (SPECT) imaging.<sup>2,3,5–10</sup> On the other hand, silver radioisotopes, including silver-103 (<sup>103</sup>Ag,  $t_{1/2}$  = 65.7 min) and silver-111 (<sup>111</sup>Ag,  $t_{1/2}$  = 7.45 d), have recently attracted interest for their theranostic potential despite being less explored.<sup>1,5,11–15</sup> These radioisotopes offer decay profiles suitable for  $\beta^-$  therapy and associated SPECT (<sup>111</sup>Ag) or PET (<sup>103</sup>Ag) imaging modalities.<sup>1</sup>

A major challenge in the development of group 11-based theranostic radiopharmaceuticals lies in designing chelators that can form thermodynamically stable and kinetically inert complexes with both copper and silver ions under physiological conditions.<sup>16–21</sup> Indeed, in the absence of such robust chelation, metal dissociation may occur *in vivo*, leading to uncontrolled redistribution of the radionuclide throughout the body. This can result in significant off-target toxicity, compromising patient safety and diminishing the diagnostic/therapeutic efficacy by preventing the radiation from reaching the tumor site. Developing a single ligand capable of effectively coordinating both copper and silver ions is also of strategic value, as it would enable the construction of chemically analogous radiopharmaceuticals that differ only in the choice of the radionuclide. Such a unified approach could streamline radiopharmaceutical development, simplify regulatory pathways, and offer clinicians a flexible toolkit for personalized nuclear medicine by switching between different diagnostic and therapeutic radioisotopes without altering the molecular architecture of the radiopharmaceutical.

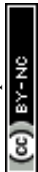
Over the past decade, a variety of chelators, such as 1,4,7,10-tetraazacyclododecane-1,4,7,10-tetraacetic acid (DOTA), 1,4,8,11-tetraazacyclotetradecane-1,4,8,11-tetraacetic acid (TETA), and their cross-bridged analogues, have been developed to accommodate the borderline Lewis acid nature of [<sup>64/67</sup>Cu]Cu<sup>2+</sup>. Nonetheless, limitations such as *in vivo* transchelation, redox instability due to Cu<sup>2+</sup> bioreduction to Cu<sup>+</sup>, and slow radiolabeling kinetics have limited their broader clinical adoption.<sup>9,22–32</sup> More promising results have been achieved with 1,4,7-triazacyclononane-1,4,7-triacetic acid (NOTA) and its bifunctional derivative (NODAGA), as well as sarcophagine-based chelators (e.g., DiamSar), which



currently represent the gold standards for  $[^{64/67}\text{Cu}]\text{Cu}^{2+}$  binding.<sup>8</sup> However, these chelators are poorly suited for  $\text{Ag}^+$ , which prefers softer donor atoms compared to  $\text{Cu}^{2+}$ .<sup>33</sup> Designing effective ligands for  $\text{Ag}^+$  remains especially demanding due to its high lability and strong tendency toward ligand exchange reactions. In fact, despite the growing interest in silver radioisotopes for theranostic applications, the coordination (radio)chemistry of  $\text{Ag}^+$  remains largely unexplored, highlighting the need for further systematic studies.<sup>34–37</sup>

In response to these challenges, in recent years, our research group has focused on developing chelators for soft (radio)metals.<sup>38–46</sup> In particular, we previously synthesized and characterized a library of sulfur-rich macrocyclic ligands tailored to the coordination preferences of group 11 metals (**Figure 1** and **Figure S1**).<sup>38–44,47</sup> These ligands exhibited high affinity for both  $\text{Cu}^{2+/+}$  and  $\text{Ag}^+$ , even under highly dilute radiochemical conditions. Among them, 1,7-bis[2-(methylsulfanyl)ethyl]-1,4,7,10-tetraazacyclododecane-4,10-diacetic acid (DO2A2S) emerged as the top-performing candidate for copper radioisotopes, while 1,4,7,10-tetrakis[2-(methylsulfanyl)ethyl]-1,4,7,10-tetraazacyclododecane (DO4S) showed the best performance for silver radionuclides.<sup>41,43</sup> However, the  $[^{111}\text{Ag}][\text{Ag}(\text{DO4S})]^+$  complex demonstrated limited stability in human serum, undergoing a noticeable degradation within a few hours.<sup>43</sup> While this may still be acceptable for proof-of-concept preclinical investigations with short-lived Ag radioisotopes (e.g.,  $^{103}\text{Ag}$ ), it highlights the need for improved chelation strategies for this metal ion, especially for longer imaging windows or therapeutic use.

To overcome these limitations and develop a single versatile platform for the chelation of group 11 radiometals, in the present study we designed a novel octadentate macrocycle, namely 1,7-bis[2-(methylsulfanyl)ethyl]-4,10-bis[(pyridin-2-yl)methyl]-1,4,7,10-tetraazacyclododecane (DO2S2Py) (**Figure 1**). The choice of a cyclen (cy) backbone was driven by our previous comparative studies, in which cyclen-based ligands outperformed those containing different macrocyclic cores (**Figure 1** and **Figure S1**) in terms of stability and coordination efficiency with both  $\text{Cu}^{2+/+}$  and  $\text{Ag}^+$ .<sup>38–40,42,43</sup> We retained the two opposite sulfur-containing pendant arms, as they had previously shown a fundamental role in the metal coordination.<sup>38–40,42,43</sup> To enhance complex robustness, we inserted two pyridine (py) moieties in the trans (1,7-*N,N'*-) positions. These moieties were selected for their known affinity for copper and silver, and their steric bulkiness, which we hypothesized would help to enforce a more spatially shielded coordination environment.<sup>48–51</sup> This conformational constraint is expected to benefit the kinetic stabilization of the metal center, in particular  $\text{Ag}^+$  (the more labile metal ion), by reducing the susceptibility of the complex to dissociation or transchelation by endogenous biomolecules.



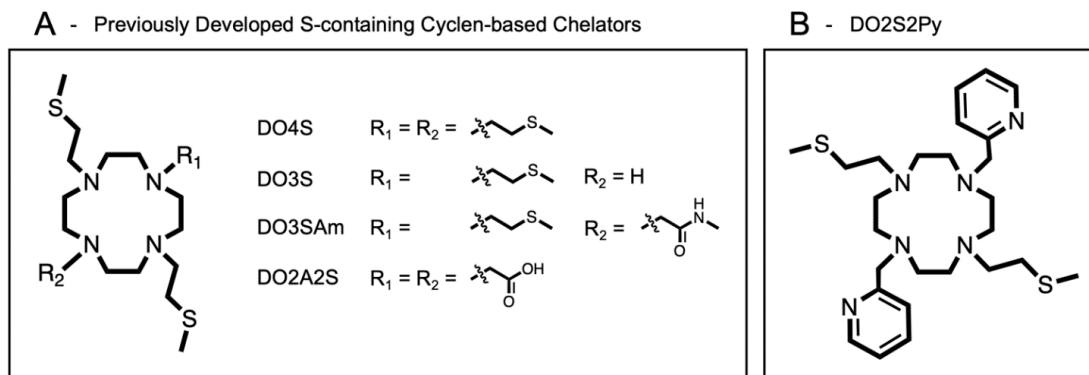


**Figure 1.** Chemical structures of (A) previously developed sulfur-containing cyclen-based chelators for copper and silver radioisotopes and (B) the chelator investigated in this work; DO2S2Py is shown in its neutral, completely deprotonated, form.

In this work, we report the synthesis and a comprehensive theoretical and experimental evaluation of DO2S2Py as a chelator for both copper and silver radioisotopes for nuclear medicine applications. We investigated its solution behavior, determined the thermodynamic stability constants, studied the complexation and decomplexation kinetics, and elucidated the solution structures of its  $\text{Cu}^{2+}$  and  $\text{Ag}^+$  complexes. The ability of DO2S2Py to bind  $[\text{}^{64}\text{Cu}]\text{Cu}^{2+}$  and  $[\text{}^{111}\text{Ag}]\text{Ag}^+$  under extremely diluted radiochemical conditions was also assessed and complemented with the evaluation of the *in vitro* stability of the corresponding radioactive complexes in biological environment, a pillar requirement for further *in vivo* applications.

## 2. Results and Discussion

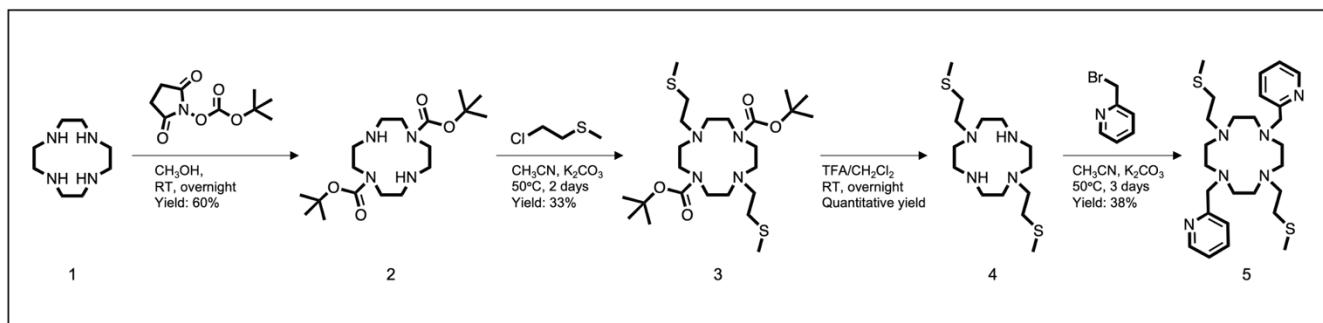
### 2.1. Synthesis of DO2S2Py

DO2S2Py was obtained according to the synthetic pathway illustrated in **Scheme 1**. The synthesis began with the selective protection of two opposite nitrogen atoms ( $\text{N}_1$ ,  $\text{N}_7$ ) of the cyclen ring (**1**) using N-(tert-butyloxycarbonyloxy)succinimide (Boc-OSu) in dry methanol, affording 1,7-bis(tert-butyloxycarbonyl)-1,4,7,10-tetraazacyclododecane (**2**, di-Boc-cyclen). This protection strategy was introduced to enable regioselective functionalization of the macrocycle as direct alkylation would otherwise lead to non-selective mixtures of substitution patterns. Boc protection of two nitrogen atoms allows a controlled trans-functionalization pattern in the subsequent steps.

In the second step, di-Boc-cyclen was reacted with 2-chloroethylmethyl sulfide in acetonitrile in the presence of  $\text{K}_2\text{CO}_3$  to yield 1,7-bis(tert-butyloxycarbonyl)-4,10-bis(2-(methylsulfanyl)ethyl)-1,4,7,10-tetraazacyclododecane (**3**, di-Boc-DO2S). Subsequent acidic deprotection using trifluoroacetic acid (TFA) in dichloromethane afforded 1,7-bis(2-(methylsulfanyl)ethyl)-1,4,7,10-tetraazacyclododecane as a TFA



salt (**4**, DO2S), which was then alkylated with 2-(bromomethyl)pyridine hydrobromide in acetonitrile and in presence of  $K_2CO_3$  to produce DO2S2Py (**5**). All the intermediates and DO2S2Py were fully characterized by Nuclear Magnetic Resonance ( $^1H$  NMR,  $^{13}C\{^1H\}$  NMR,  $^1H$ - $^1H$  COSY, and  $^1H$ - $^{13}C$  HSQC), and high-resolution mass spectrometry (HR-MS). The corresponding spectra are reported in **Figure S2 - S15**. The overall multistep synthesis allowed to provide the pure chelator DO2S2Py, although in low yield (8%).



**Scheme 1.** Synthesis of DO2S2Py.

## 2.2. Acid-Base Properties of DO2S2Py

Before investigating the coordination behavior of DO2S2Py toward  $Cu^{2+}$  and  $Ag^+$ , a comprehensive characterization of its acid-base properties in aqueous solution was carried out. Specifically, the acidity constants ( $pK_a$ ) of the new chelator were determined by pH-potentiometry and pH-dependent  $^1H$  NMR and UV-Vis spectroscopic titrations. Multiple complementary techniques were employed to provide independent and mutually consistent datasets. This characterization step is essential, as the protonation state of the ligand directly impacts its metal-binding ability due to the intrinsically competitive nature of protonation and metal coordination equilibria.

The  $^1H$  NMR spectra of DO2S2Py as a function of pH is shown in **Figure 2**, along with signal assignments. The methyl protons ( $H_1$ ) of the thioether arms ( $SCH_3$ ) of DO2S2Py remain almost unaffected across the investigated pH range, consistently appearing as a singlet at  $\sim 2$  ppm. This behavior is attributed to their positioning far from the proton binding sites, making them essentially insensitive to the protonation state of the molecule. In contrast, all the other proton signals display a clear pH dependence, consistent with their proximity to protonable sites. At acidic pH, the methylene protons of the sulfur-containing sidechains ( $SCH_2$  and  $NCH_2$ ,  $H_2$  and  $H_3$ ) appear as two distinct broad singlets at 2.85 and 3.35 ppm, respectively. As the pH increases, these signals shift upfield and coalesce into a single resonance at 2.50 ppm at  $pH > 12$ . A similar trend is also observed for the  $NCH_2$  protons ( $H_4$ ) of the macrocyclic ring (*i.e.* they resonate as two separate singlets at 3.60 and 3.22 ppm at pH 2, and merge



into one signal at 2.95 ppm above pH 12). The CH<sub>2</sub> protons bridging the pyridine rings and the macrocycle (H<sub>5</sub>) resonate as a singlet throughout the titration but exhibit a continuous variation in chemical shift with increasing pH. The aromatic region also displays pronounced pH-dependent changes: the pyridine protons experience progressive upfield shifts upon deprotonation while the *meta* protons (H<sub>6</sub> and H<sub>8</sub>) relative to the aromatic N coalesce into a single resonance below pH 7. The ortho (H<sub>9</sub>) and para (H<sub>7</sub>) protons remain distinct across the entire pH range. The pH-dependent chemical shift trends were fitted to derive the pK<sub>a</sub> values, reported in **Table 1**. The obtained data were corroborated by pH-potentiometric titrations (**Table 1**). The corresponding species distribution diagram is presented in **Figure S16**. These results indicate that a mixture of bi- and monoprotonated species (H<sub>2</sub>L<sup>2+</sup> and HL<sup>+</sup>) exist under physiological pH conditions.

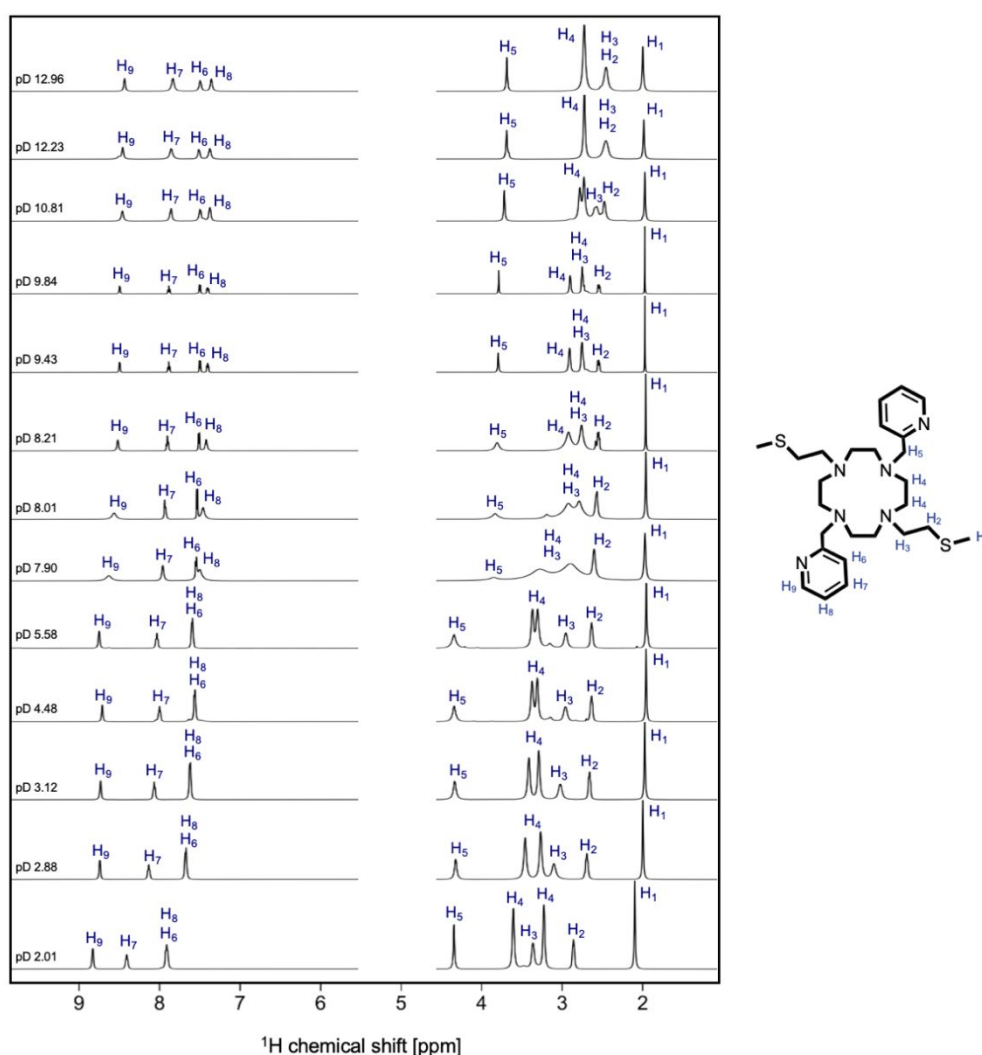


**Figure 2.** Representative <sup>1</sup>H NMR spectra of DO2S2Py at different pH values (400 MHz, D<sub>2</sub>O, T = 25°C, I = 0.15 M NaCl or 0.15 M NaNO<sub>3</sub>, C<sub>DO2S2Py</sub> = 1 · 10<sup>-3</sup> M). Note: no effect of different ionic strength was observed.



DO2S2Py is formally a hexaprotic molecule, containing four tertiary amines within the macrocyclic ring and two pyridine nitrogen atoms. However, only four  $pK_a$  values could be determined under our experimental conditions. The last two ( $pK_{a,5}$  and  $pK_{a,6}$ ) are attributed to the deprotonation of the two macrocyclic nitrogen atoms located opposite each other (**Table 1**). This assignment is supported by previous studies on cyclen-based ligands, which show preferential protonation at opposite sites to minimize electrostatic repulsion between adjacent protonated centers.<sup>47</sup> The intermediate two  $pK_a$  ( $pK_{a,3}$  and  $pK_{a,4}$ ) are ascribed to the deprotonation of the pyridine nitrogen atoms (**Table 1**). The first two protonation steps ( $pK_{a,1}$  and  $pK_{a,2}$ ), corresponding to the remaining tertiary amines of the cyclen ring, were not detected, likely due to their very low values ( $pK_a < 1$ ). These highly protonated species are typically unstable and only appreciably formed at extremely acidic pH ( $pH < 1$ ), making their detection challenging. This behavior is well-documented in the literature and is a characteristic of cyclen-based macrocycles.<sup>47,52</sup>

**Table 1.** Acidity constants ( $pK_a$ ) of DO2S2Py and overall stability constants ( $\log\beta$ ) of its  $Cu^{2+}$  and  $Ag^+$  complexes ( $I = 0.1$  M NaCl ( $Cu^{2+}$ )/ $NaNO_3$  ( $Ag^+$ ),  $T = 25^\circ C$ ) obtained with the different techniques.

	<sup>1</sup> H NMR	Potentiometry	UV-Vis
<b>Equilibria</b> (a)		<b><math>pK_a</math></b>	
$HL^+ \rightleftharpoons L + H^+$	$10.76 \pm 0.03$	$10.8 \pm 0.1$	-
$H_2L^{2+} \rightleftharpoons HL^+ + H^+$	$7.75 \pm 0.09$	$7.82 \pm 0.05$	$7.78 \pm 0.1$
$H_3L^{3+} \rightleftharpoons H_2L^{2+} + H^+$	$3.10 \pm 0.06$	$3.19 \pm 0.05$	$3.33 \pm 0.02$
$H_4L^{4+} \rightleftharpoons H_3L^{3+} + H^+$	$2.6 \pm 0.1$	-	$2.53 \pm 0.02$
<b>Equilibria</b> (a)		<b><math>\log\beta</math></b>	
$Cu^{2+} + L \rightleftharpoons [CuL]^{2+}$	-	-	$23.62 \pm 0.07$
$Ag^+ + L \rightleftharpoons [AgL]^+$	$16.94 \pm 0.08$	$16.83 \pm 0.04$	-
$Ag^+ + HL \rightleftharpoons [AgHL]^{2+}$	$20.64 \pm 0.05$	$20.6 \pm 0.1$	-
$Ag^+ + L + H_2O \rightleftharpoons [AgL(OH)] + H^+$	$6.65 \pm 0.09$	$6.6 \pm 0.1$	-

(a) L represents the completely deprotonated form of DO2S2Py as shown in **Figure 1**. The reported uncertainty was obtained by the fitting procedure and represents one standard deviation unit.

The  $pK_a$  values associated with the macrocyclic amine groups of DO2S2Py closely resemble those previously reported for sulfur-containing analogues such as DO4S, as well as for pyridine-functionalized derivatives including cyclen-1Py, cyclen-2Py, and cyclen-4Py (**Table S1**).<sup>47,50,51</sup> Similarly, the  $pK_a$  values attributed to the pyridine moieties of DO2S2Py are in good agreement with those of related ligands bearing only pyridine substituents (**Table S1**).<sup>50,51</sup> This indicates that the presence of the sulfanyl side chains does not significantly perturb the protonation behavior of the pyridine nitrogen atoms, suggesting minimal electronic/steric influence on their basicity.



The protonation constants determined by  $^1\text{H}$  NMR spectroscopy were further corroborated through pH-dependent UV-Vis spectrophotometric titrations. Representative pH-dependent electronic spectra of DO2S2Py are shown in **Figure S17**. The UV-Vis spectrum of DO2S2Py exhibits electronic transitions originating from both the aliphatic sulfur-containing macrocyclic core, which gives rise to absorption bands below 250 nm, and the pyridine rings, characterized by a distinct absorption maximum centered at 262 nm. The latter band closely resembles that observed for the monopyridine-functionalized cyclen analogue (cyclen-Py), suggesting that it can be attributed to the  $\pi$ - $\pi^*$  transitions of the pyridine moieties.<sup>50</sup> Systematic pH-dependent variations in the electronic absorption spectra enabled the determination of the acidity constants of the ligand ( $pK_{a,2}$ ,  $pK_{a,3}$ , and  $pK_{a,4}$ ), which are summarized in **Table 1**. Notably, these values are in excellent agreement with those obtained with other techniques.

### 2.3 Kinetics of DO2S2Py Complexes Formation

Before evaluating the thermodynamic stability of the  $\text{Ag}^+$  and  $\text{Cu}^{2+}$  complexes of DO2S2Py, the formation kinetics of these species were qualitatively investigated.

**2.3.1.  $\text{Cu}^{2+}$ -DO2S2Py.** In the case of  $\text{Cu}^{2+}$ , kinetic studies were performed by UV-Vis spectroscopy at different pH values (pH 2, 4.5, and 7). Representative spectra are reported in **Figure S18**. In all cases, the addition of  $\text{Cu}^{2+}$  to the ligand solution induced an immediate change in the electronic spectra of DO2S2Py. Notably, an enhanced absorbance at wavelengths beyond the absorption maximum ( $> 270$  nm), along with a broad band centered around 677 nm, was observed compared to the free ligand (**Figure S18** and **Figure S19**). No significant spectral changes were detected over time. These data provide clear evidence of complex formation under the investigated pH conditions. Moreover, these findings indicate that DO2S2Py coordinates  $\text{Cu}^{2+}$  instantaneously across the investigated pH range, regardless of the protonation state of the ligand. This behavior is in contrast with previous observations for structurally analogous sulfur-containing chelators lacking pyridine moieties (DO4S, DO3S and DO3SAm, **Figure 1**), where markedly slower complexation kinetics were observed at progressively more acidic pH due to increased electrostatic repulsion between the dicationic  $\text{Cu}^{2+}$  ion and highly protonated ligand species.<sup>38</sup> For example, in the case of DO4S, complexation at pH 2 required up to 10 days to reach equilibrium (**Table S2**).<sup>38</sup> The significantly enhanced formation kinetics observed for DO2S2Py highlight the key role played by the pyridine groups in accelerating the complexation event.

**2.3.2.  $\text{Ag}^+$ -DO2S2Py.** A similar behavior was observed for  $\text{Ag}^+$ : the addition of the metal ion to a solution of DO2S2Py induced immediate and distinct changes in the  $^1\text{H}$  NMR spectra compared to the free ligand (**Figure S20**), consistent with the rapid formation of  $\text{Ag}^+$ -DO2S2Py complexes. These spectral modifications occurred without any detectable time evolution, indicating that complexation reaches equilibrium faster than the timescale of experimental acquisition. Notably, such fast complexation kinetics



with  $\text{Ag}^+$  are consistent with previous observations for related S-rich chelators in the absence of pyridine units, suggesting that silver coordination is inherently more rapid and less sensitive to the nature of the auxiliary donor groups compared to  $\text{Cu}^{2+}$ .<sup>42,43</sup>

## 2.4 Thermodynamic Stability of DO2S2Py Complexes

The stability constants ( $\log\beta$ ) of  $\text{Cu}^{2+}$ -DO2S2Py and  $\text{Ag}^+$ -DO2S2Py complexes were determined using UV-Vis ( $\text{Cu}^{2+}$ ),  $^1\text{H}$  NMR ( $\text{Ag}^+$ ) spectroscopic titrations as well as potentiometry ( $\text{Cu}^{2+}$  and  $\text{Ag}^+$ ).

**2.4.1  $\text{Cu}^{2+}$ -DO2S2Py.** Representative electronic spectra of  $\text{Cu}^{2+}$ -DO2S2Py recorded at various pH values and the corresponding pH-dependent absorbance profile at a selected wavelength are presented in **Figure S21**.

No significant spectral changes were observed in the pH range 3-12, indicating that the speciation remains constant across this range and that a single  $\text{Cu}^{2+}$ -containing species predominates. In contrast, at  $\text{pH} < 3$ , a marked decrease in absorbance was noted, and the spectral features increasingly resembled those of the free ligand (compare **Figure 2** with **Figure S21**). This behavior is consistent with proton-induced dissociation of the complex and the release of the uncoordinated ligand occurring at highly acidic media ( $\text{pH} < 2$ ). These spectroscopic data were fitted using a suitable equilibrium model, yielding the stability constant reported in **Table 1**. According to the derived speciation, DO2S2Py forms a single mononuclear complex with  $\text{Cu}^{2+}$ , namely  $[\text{CuL}]^{2+}$ . The stoichiometry of the complex was further confirmed by pH-potentiometry and mass spectrometry (**Figure S22**). The latter revealed a single peak corresponding to the 1:1 metal-to-ligand species, with no evidence of polynuclear aggregates. The corresponding speciation diagram is presented in **Figure 3**.

Interestingly, compared to previously developed sulfur-containing analogues (e.g., DO4S), the  $\text{Cu}^{2+}$  complexation behavior of DO2S2Py is identical in terms of speciation: in all cases, only the fully deprotonated mononuclear species is formed.<sup>38</sup> This suggests that the presence of the pyridine moiety does not alter the speciation profile. The formation of protonated species appears disfavored, likely due to the neutral nature of the ligand, which would lead to highly charged complexes ( $[\text{CuHL}]^{3+}$ ,  $[\text{CuH}_2\text{L}]^{4+}$  etc.). The speciation model is also consistent with that of  $\text{Cu}^{2+}$ -cyclen-1Py but differs from that of  $\text{Cu}^{2+}$ -cyclen-2Py, where additional species such as the monoprotonated complex ( $[\text{CuHL}]^{3+}$ ) and a hydroxo-containing complex ( $[\text{CuL}(\text{OH})]^+$ ) were observed (however, in this case, a different supporting electrolyte was used, i.e.  $\text{NMe}_4\text{NO}_3$ ).<sup>50,51</sup>



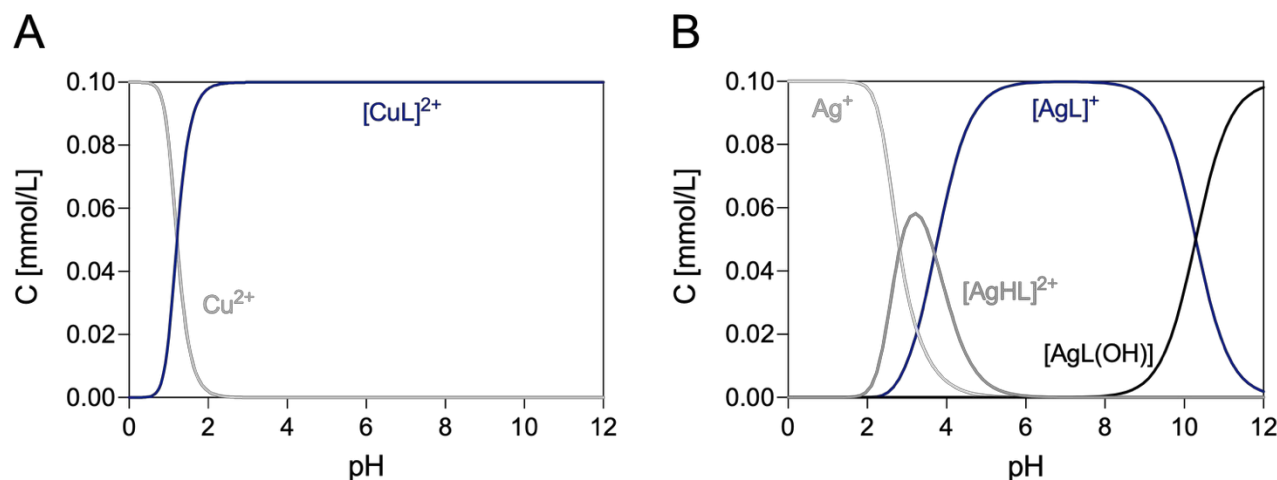


**Figure 3.** Distribution diagrams of (A)  $\text{Cu}^{2+}$ -DO2S2Py and (B)  $\text{Ag}^{+}$ -DO2S2Py ( $C_{\text{DO2S2Py}} = 1 \cdot 10^{-4}$  M,  $C_{\text{M}} = 1 \cdot 10^{-4}$  M,  $\text{M} = \text{Cu}^{2+}$  or  $\text{Ag}^{+}$ ).

**2.4.2  $\text{Ag}^{+}$ -DO2S2Py.** The  $^1\text{H}$  NMR spectra of  $\text{Ag}^{+}$ -DO2S2Py recorded at different pH values are shown in **Figure S23** (the signal attribution was performed with the aid of 2D homo- and hetero-correlated NMR experiments; representative 2D spectra are reported in **Figure S24** and **Figure S25**). These spectra differ markedly from that of the free ligand (**Figure 2**), indicating successful metal coordination throughout the investigated pH range.

At pH values above 11, the  $^1\text{H}$  NMR spectra are invariant, suggesting the predominance of a single species. Similarly, in the pH range 5-8, the  $^1\text{H}$  NMR spectra remain unchanged, implying the existence of a second complex. Below pH 4, additional spectral changes are observed, consistently with the presence of other species. The pronounced pH sensitivity of the spectra supports the presence of multiple, pH-dependent complexes differing in their protonation state, as also indicated by pH-potentiometry. The obtained  $^1\text{H}$  NMR and pH-potentiometric data were fitted to a suitable equilibrium model, from which the stability constants of the complexes were derived (**Table 1**). According to the proposed speciation model, DO2S2Py forms exclusively 1:1 metal-to-ligand complexes, namely  $[\text{AgHL}]^{2+}$ ,  $[\text{AgL}]^{+}$  and  $[\text{AgL}(\text{OH})]$ . The corresponding species distribution diagram is reported in **Figure 3**. As with  $\text{Cu}^{2+}$ , the speciation model determined for  $\text{Ag}^{+}$ -DO2S2Py closely resembles those previously reported for analogous sulfur-containing chelators.<sup>42,43</sup> The only notable difference is the detection of a hydroxo complex with this ligand, which was not observed for other cyclen-based chelators. The differences observed between  $\text{Ag}^{+}$  and  $\text{Cu}^{2+}$  also reflect previous findings, where the lower charge of  $\text{Ag}^{+}$  had shown to favor the formation of more protonated species.<sup>38,42</sup>

**2.4.3 Stability Comparisons.** To enable a meaningful comparison of complex stability across systems involving ligands with different basicity, metal ions with distinct hydrolysis behavior, or complexes with



varying stoichiometries, it is essential to calculate pM values. Defined as  $pM = -\log [M]_{\text{free}}$ , where  $[M]_{\text{free}}$  is the concentration of unbound metal ion at equilibrium, this parameter offers a standardized and practical metric of the effective metal-binding affinity of a ligand under biologically relevant conditions.<sup>53</sup> Indeed, unlike stability constants ( $\log K$ ), pM values account for proton competition and metal hydrolysis, enabling direct and quantitative comparisons between different systems.

The high values observed for the  $pCu^{2+}$  and  $pAg^+$  of DO2S2Py indicate that the ligand exhibits strong affinity toward both metal ions (**Figure 4**).

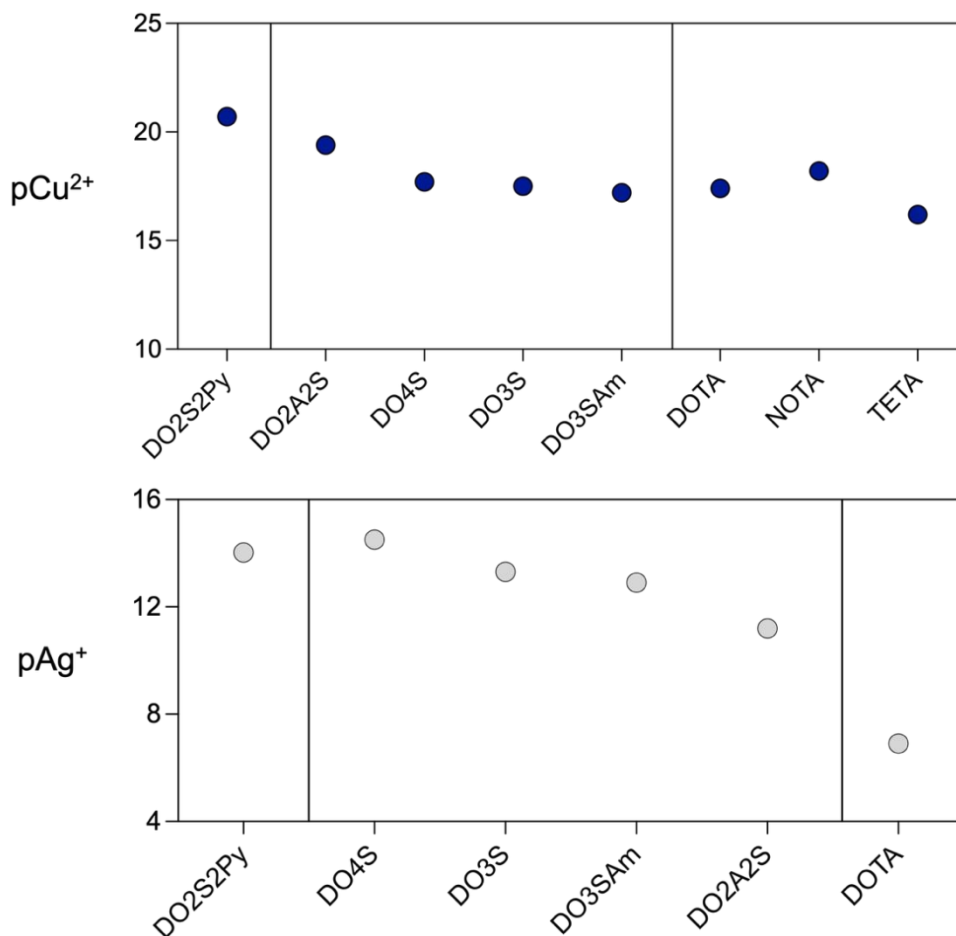


**Figure 4.** Comparison of  $pCu^{2+}$  and  $pAg^+$  values of the  $Cu^{2+}$  and  $Ag^+$  complexes formed with DO2S2Py and various state-of-the-art chelators.  $pCu^{2+}$  and  $pAg^+$  values were calculated at pH 7.4 and  $C_{DO2S2Py} = 1 \cdot 10^{-5} M$ ,  $C_M = 1 \cdot 10^{-6} M$  ( $M = Cu^{2+}$  or  $Ag^+$ ).

When benchmarked against the sulfur-containing chelators previously developed (e.g., DO4S and DO2A2S), as well as clinically established ligands like NOTA and DOTA, DO2S2Py exhibits exceptional affinity for  $Cu^{2+}$  (**Figure 4**).<sup>38</sup> In particular, its  $pCu^{2+}$  value ( $pCu^{2+} = 20$ ) exceeds that of DO2A2S ( $pCu^{2+} = 19.4$ ), previously identified as our best-performing S-rich  $Cu^{2+}$  chelator, as well as those of NOTA ( $pCu^{2+} = 18.2$ ), DOTA ( $pCu^{2+} = 17.4$ ) and TETA ( $pCu^{2+} = 16.2$ ).<sup>38</sup> Notably, compared to other cyclen-based



pyridine-containing ligands (e.g., cyclen-2Py and cyclen-1Py), DO2S2Py consistently forms more stable  $\text{Cu}^{2+}$  complexes (**Figure S26**).<sup>50,51</sup> This enhancement in stability suggests that the simultaneous presence of soft (S) and borderline (N) donor atoms allows us to fine-tune the ligand's coordination environment improving metal binding. Regarding  $\text{Ag}^+$ , the complex formed with DO2S2Py exhibits thermodynamic stability nearly identical ( $\text{pAg}^+ = 14$ ) to  $\text{Ag}^+$ -DO4S ( $\text{pCu}^{2+} = 14.5$ ), the current benchmark chelator for silver radioisotopes (**Figure 4**).<sup>42</sup> These results underscore the versatility of DO2S2Py as a chelator capable of effectively coordinating these metal ions despite their different coordination preferences, highlighting its potential for radiopharmaceutical applications.

## 2.5 Structure of DO2S2Py Complexes in Aqueous Environment

The coordination geometries of  $\text{Cu}^{2+}$ -DO2S2Py and  $\text{Ag}^+$ -DO2S2Py in aqueous environment were investigated using a multifaceted theoretical and experimental approach that combined NMR ( $\text{Ag}^+$ ), Electron Paramagnetic Resonance (EPR,  $\text{Cu}^{2+}$ ) and UV-Vis ( $\text{Cu}^{2+}$ ) spectroscopies with Density Functional Theory (DFT) calculations ( $\text{Cu}^{2+}$  and  $\text{Ag}^+$ ).

**2.5.1  $\text{Cu}^{2+}$ -DO2S2Py.** Frozen solution EPR spectra of  $\text{Cu}^{2+}$ -DO2S2Py mixtures at varying pH values are presented in **Figure 5**. These data indicate that, across the investigated pH range (2-10), only a single predominant complex exists (i.e.  $[\text{CuL}]^{2+}$ ), in addition to the  $\text{Cu}^{2+}$ -aqua complex, supporting the conclusions drawn from UV-Vis spectroscopy and potentiometry. No protonated, mixed hydroxo-complexes, or other geometrical isomers could be observed by EPR.

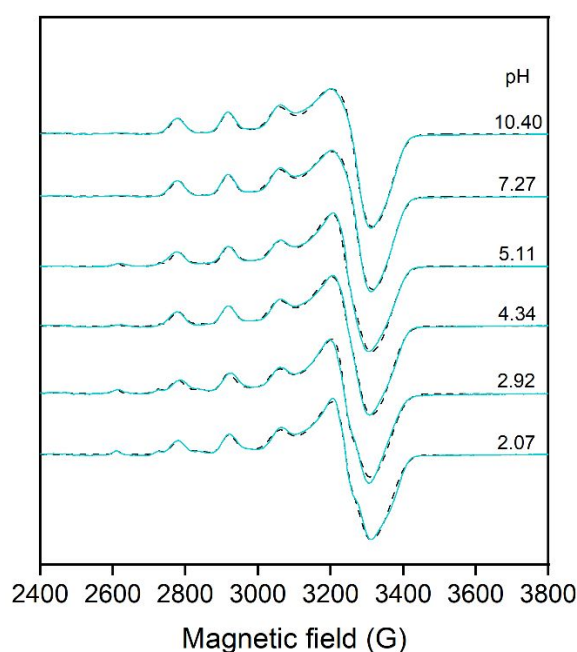


**Figure 5.** Measured (black) and simulated (blue) frozen EPR spectra of  $\text{Cu}^{2+}$ -DO2S2Py at different pH.



The EPR spectrum of  $[\text{Cu}(\text{DO2S2Py})]^{2+}$  in frozen solution is notably broad (**Figure 5**) and could be described with parameters  $g_{\perp}=2.067$ ,  $g_{\parallel}=2.248$ , and  $A_{\parallel}=144 \cdot 10^{-4} \cdot \text{cm}^{-1}$ . Due to the broad perpendicular line, approximate axial  $g$ - and  $A$ -tensors could be simulated (**Table 2**), with considerable uncertainty in the perpendicular components. This pronounced broadening is likely the result of rhombic distortion in the coordination geometry, indicating a deviation from axial symmetry.

In **Table S3**, the EPR parameters of several relevant  $\text{Cu}^{2+}$  macrocyclic complexes are compared with the values obtained in the present study.<sup>38,51</sup> Based on this comparison, 4N and 4NS coordination modes can be excluded, as these typically exhibit significantly smaller  $g_{\parallel}$  values and larger  $A_{\parallel}$  values than those observed for  $[\text{Cu}(\text{DO2S2Py})]^{2+}$ . Instead, the parameters are closer to those reported for DO2A2S, in which two carboxylate side chains and two ring nitrogens occupy the equatorial plane, while the remaining two macrocyclic nitrogens are located farther from the metal center in axial positions.<sup>38</sup>

A similar coordination mode can be envisaged for  $\text{Cu}^{2+}$ -DO2S2Py if the pyridine nitrogens coordinate in place of the carboxylate groups. In this case, the pyridine donors would be displaced slightly above and below the equatorial plane to minimize steric repulsion between them. The somewhat smaller  $g_{\parallel}$  values observed in our spectra are also consistent with this model, reflecting the stronger ligand field exerted by nitrogen donors compared to oxygen. Such geometry has also been confirmed by single-crystal X-ray diffraction for  $[\text{Cu}(\text{CRpy}_2)]^{51}$ , whose EPR parameters reported in frozen DMF solvent (150 K) were found to be close to those measured for  $[\text{Cu}(\text{DO2S2Py})]^{2+}$ . Deviations from an ideal elongated octahedral geometry (e.g., donor atoms bound to copper ions deviate from the equatorial plane or the axial donor groups forming angles smaller than  $90^\circ$  with the equatorial plane) contribute to strong rhombicity and the resulting spectral broadening.

**Table 2.** EPR parameters obtained by the simulation of EPR spectra of  $[\text{Cu}(\text{DO2S2Py})]^{2+}$  in frozen solution.

Anisotropic parameters <sup>(a)</sup>							$g_{0,\text{calc}}$ <sup>(b)</sup>
$g_x$	$g_y$	$g_z$	$A_x$ / $10^{-4} \text{ cm}^{-1}$	$A_y$ / $10^{-4} \text{ cm}^{-1}$	$A_z$ / $10^{-4} \text{ cm}^{-1}$		
2.067	2.067	2.248	12	12	144	2.127	

<sup>a</sup> The experimental errors were  $\pm 0.002$  for  $g_x$  and  $g_y$  and  $\pm 0.001$  for  $g_z$ ,  $\pm 2 \cdot 10^{-4} \text{ cm}^{-1}$  for  $A_x$  and  $A_y$  and  $\pm 1 \cdot 10^{-4} \text{ cm}^{-1}$  for  $A_z$ .

<sup>b</sup> Calculated with the equation  $g_{0,\text{calc}} = (g_x + g_y + g_z)/3$ .

The EPR spectrum of  $[\text{Cu}(\text{DO2S2Py})]^{2+}$  at room temperature (**Figure S27**) can be simulated by averaging the anisotropic parameters obtained from the frozen-state analysis. As in the frozen spectrum, the room temperature signal is also extremely broad, which is partly due to the relatively small copper hyperfine coupling constant. In addition, the rotational correlation time of  $4.2 \cdot 10^{-10} \text{ s}$  suggests slow molecular



tumbling, likely caused by steric hindrance from the non-coordinating side arms, which impede rotational motion.

To obtain further insights into the structures of the complexes formed by coordination of the DO2S2Py ligand, quantum mechanical DFT calculations were performed. All the relevant coordination geometries of DO2S2Py with Cu<sup>2+</sup>, as well as Cu<sup>+</sup> and Ag<sup>+</sup>, were explored to identify the preferred coordination modes for each metal ion and to rationalize the experimentally observed behavior. The fully deprotonated form of DO2S2Py was considered in all the calculations.

Based on our simulations, the most stable structures were obtained when the metal was inserted into the cavity of the DO2S2Py ligand. All the optimized structures of the Cu<sup>2+</sup> metal complexes are shown in **Figure S28** along with their Gibbs free energies ( $\Delta G$ ) calculated in water (**Table 3**). The most important distances between the ligand and the metals are reported in **Table S4**.

**Table 3.** Gibbs free energies ( $\Delta G$ ) calculated in water for the different coordination modes of the Cu<sup>2+</sup>, Cu<sup>+</sup>, and Ag<sup>+</sup> complexes of DO2S2Py.

Metal ion	Coordination mode	$E$ [kcal·mol <sup>-1</sup> ]
Cu <sup>2+</sup>	4N <sub>cy</sub> 2N <sub>py</sub>	-34.3
	4N <sub>cy</sub> 1N <sub>py</sub>	-32.9
	4N <sub>cy</sub>	-31.9
	4N <sub>cy</sub> 1S	-25.2
Cu <sup>+</sup>	3N <sub>cy</sub> 1N <sub>py</sub>	-26.1
	3N <sub>cy</sub> 1S	-24.2
	4N <sub>cy</sub>	-23.2
Ag <sup>+</sup>	4N <sub>cy</sub> 1N <sub>py</sub> 1S	-21.7
	4N <sub>cy</sub> 2N <sub>py</sub>	-21.3
	4N <sub>cy</sub> 2S	-17.5

Upon coordination of Cu<sup>2+</sup>, all the computed structures exhibit high stability, indicating that the ligand has a strong affinity for the metal center, in agreement with experimental observations. The most stable structure is obtained when the Cu<sup>2+</sup> cation is placed in the middle of the macrocycle but slightly displaced above the cavity, forming strong coordination bonds with three nitrogen atoms of the macrocyclic core (N<sub>cy</sub>) and with the two pyridine nitrogen atoms (N<sub>py</sub>). A weaker interaction is established with the fourth nitrogen atom of the macrocycle. This coordination mode is denoted as [Cu<sup>2+</sup>-4N<sub>cy</sub>2N<sub>py</sub>]. The resulting coordination geometry confirms experimental findings of a distorted elongated octahedral arrangement, with the two pyridine nitrogens lying within the equatorial plane, whereas two nitrogen atoms of the macrocycle occupy the axial position.

The calculated electronic spectrum for this configuration closely reproduces the experimental one reported in **Figure S18**. The optimized structure of the [Cu<sup>2+</sup>-4N<sub>cy</sub>2N<sub>py</sub>] complex, together with its UV-Vis spectrum, computed using the same theoretical protocol, is reported in **Figure 6**. The electronic



transitions describing the absorption spectrum were fully characterized and are collected in **Table S5**. The Gibbs free energy calculated for the formation of  $[\text{Cu}^{2+}-4\text{N}_{\text{cy}}2\text{N}_{\text{py}}]$  species is  $-34.3 \text{ kcal}\cdot\text{mol}^{-1}$  (**Table 3**), corresponding to a  $\log\beta$  value of 25.1. This calculated value is in surprisingly good agreement with the experimental  $\log\beta$  of  $23.6 \pm 0.07$  (**Table 1**).

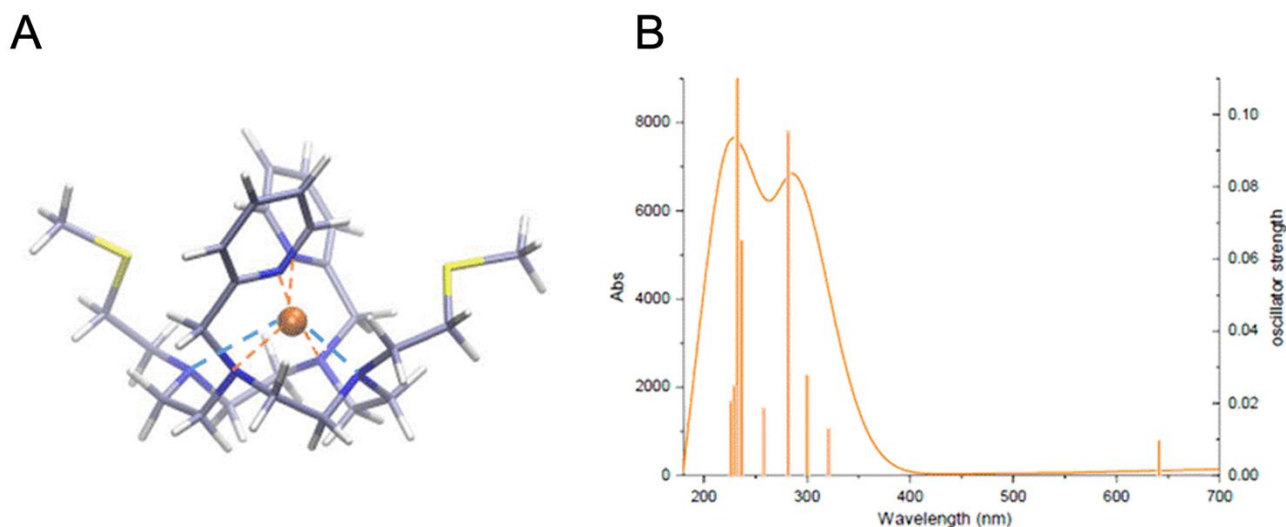


**Figure 6.** A) DFT optimized geometry of the most stable structure of  $[\text{Cu}(\text{DO}2\text{S}2\text{Py})]^{2+}$ , namely  $[\text{Cu}^{2+}-4\text{N}_{\text{cy}}2\text{N}_{\text{py}}]$  and B) the corresponding calculated TDDFT absorption spectrum.

For the geometry denoted as  $[\text{Cu}^{2+}-4\text{N}_{\text{cy}}1\text{N}_{\text{py}}]$ , in which the metal, lying in the center of the cyclen backbone, is simultaneously coordinated to the four ring nitrogen atoms and one pyridine ligand, the calculated free energy is  $-32.9 \text{ kcal}\cdot\text{mol}^{-1}$  (**Table 3**), corresponding to a  $\log\beta$  value of 24. DFT calculations, therefore, do not completely rule out the coexistence of multiple stable coordination modes of the ligand in aqueous solution.

A third stable complex was computationally identified, indicated as  $[\text{Cu}^{2+}-4\text{N}_{\text{cy}}1\text{S}]$ , that exhibits a Gibbs free energy of formation of  $-25.2 \text{ kcal}\cdot\text{mol}^{-1}$  (**Table 3**) and a corresponding  $\log\beta$  value of 18.5. Unlike the species described previously, this complex involves the coordination of one of the sulfur atoms from the pendant arms, which results in an evident minor stability. The soft character of the sulfur atom, and its lower  $\sigma$ -donation ability compared to nitrogen-based donors, likely contribute to the lower affinity of this ligand toward the  $\text{Cu}^{2+}$  metal ion. In the fourth and least stable configuration,  $[\text{Cu}^{2+}-4\text{N}_{\text{cy}}]$ , all pendant arms of DO2S2Py are oriented away from the metal center, leaving  $\text{Cu}^{2+}$  coordinated exclusively to the four nitrogen atoms of the macrocyclic cavity. This geometry can be classified as a pseudo square-planar arrangement with no axial donor interactions. The calculated Gibbs free energy for this species is  $-31.9 \text{ kcal}\cdot\text{mol}^{-1}$  (**Table 3**), corresponding to a  $\log\beta$  value of 23.4. For all the optimized structures, the calculated



Gibbs free energies indicate a good stability of the formed complexes, and all the corresponding electronic spectra were calculated. Among them, only the spectrum of the complex named  $[\text{Cu}^{2+}-4\text{N}_{\text{cy}}2\text{N}_{\text{py}}]$ , reported in **Figure 6**, closely matches the experimental one.

**2.5.2  $\text{Ag}^+-\text{DO2S2Py}$ .** Differently from the  $\text{Cu}^{2+}$  system, in presence of  $\text{Ag}^+$ , NMR is a powerful technique to elucidate chemical structure in solution. In the  $^1\text{H}$  NMR spectrum of  $[\text{Ag}(\text{DO2S2Py})]^+$ , the aliphatic protons ( $\text{H}_1$ ,  $\text{H}_2$ ,  $\text{H}_3$ , and  $\text{H}_4$ ) appear as extremely broad singlets, while the aromatic protons show the expected multiplicities: doublets for  $\text{H}_6$  and  $\text{H}_9$  and triplets for  $\text{H}_7$  and  $\text{H}_8$  (**Figure 7**). Each set of chemically equivalent protons giving rise to a single resonance indicates that the opposite side arms, which are identical in structure, are also magnetically equivalent in solution upon metal coordination.

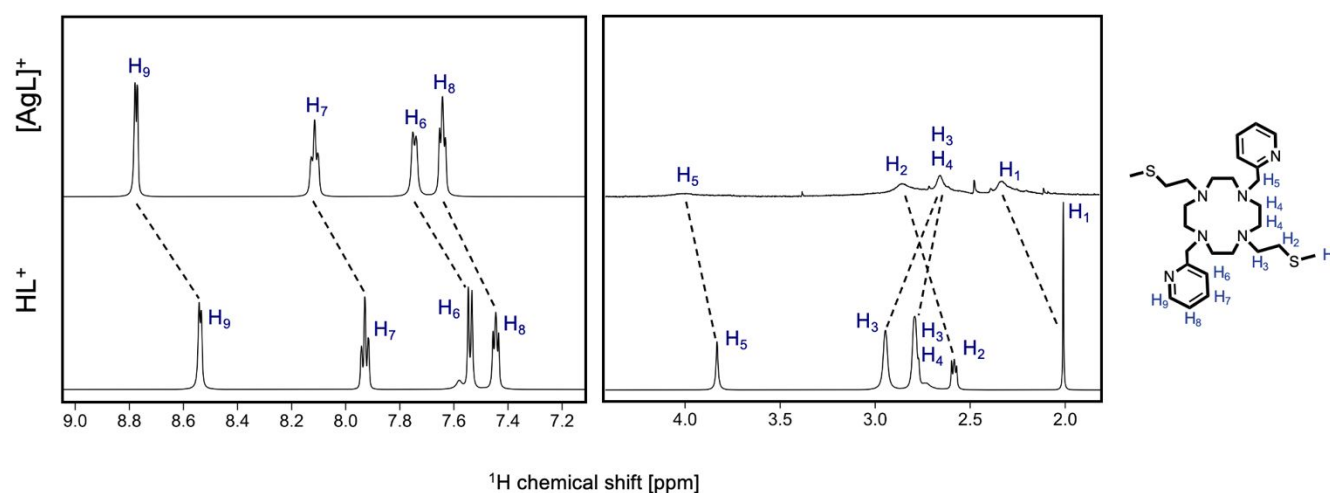


**Figure 7.** Comparison of  $^1\text{H}$  NMR spectra of  $[\text{Ag}(\text{DO2S2Py})]^+$  and free  $\text{DO2S2Py}$  ( $\text{HL}^+$  form) (400 MHz,  $\text{D}_2\text{O}$ ,  $T = 25^\circ\text{C}$ ).

Comparison of the  $^1\text{H}$  NMR spectrum of  $[\text{Ag}(\text{DO2S2Py})]^+$  with that of the free ligand bearing the same net charge ( $\text{HL}^+$ ) provides important insights into the solution structures of this complex (**Figure 7**). The pyridine protons ( $\text{H}_6$ - $\text{H}_9$ ) are consistently deshielded in  $[\text{Ag}(\text{DO2S2Py})]^+$  compared to the free ligand. A similar downfield shift is observed for the  $\text{SCH}_3$  and  $\text{SCH}_2$  protons ( $\text{H}_1$  and  $\text{H}_2$ ) and the  $\text{NCH}_2$  protons connecting the cyclen backbone to the pyridine arms ( $\text{H}_5$ ). In contrast, the aliphatic N-bound protons on the macrocyclic backbone ( $\text{H}_3$  and  $\text{H}_4$ ) experience an overall upfield shift. These variations are consistent with coordination-induced electronic effects: deshielding near the metal due to its electron-withdrawing nature and shielding on the nitrogen-bound protons due to increased electron density upon metal coordination. Indeed, in the free ligand, protonation is localized on the amines, which leads to relatively lower electron density in these protons. In contrast, in the complexes,  $\text{Ag}^+$  likely interacts simultaneously with both nitrogen and sulfur donors, redistributing electron density and shielding the N-bound protons.



Similar trends have been previously reported for  $\text{Ag}^+$  complexes of analogous sulfur-containing ligands.<sup>42,43</sup>

Collectively, the combination of chemical shift changes and the presence of single resonances for each set of chemically equivalent protons of  $[\text{Ag}(\text{DO2S2Py})]^+$  indicates that all donors are, on average, involved in the metal binding. The data further suggests a dynamic binding regime, in which the donor atoms undergo rapid binding-unbinding events. In particular, the sulfur-containing side arms appear to experience relatively slow-exchange dynamics, as evidenced by their very broad resonances (almost approaching coalescence), whereas the pyridine donors are in fast exchange, resulting in averaged and relatively sharp signals. This fluxional behavior highlights that a flexible coordination mode is favored when  $\text{Ag}^+$  is confined in a highly dentate macrocyclic scaffold, as previously observed with similar systems.<sup>42,43</sup>

To support NMR data and clarify coordination geometry of  $\text{Ag}^+$ , DFT computations were performed. **Figure S29** reports all the optimized molecular structures for  $[\text{Ag}(\text{DO2S2Py})]^+$ , along with their corresponding Gibbs free energies ( $\Delta G$ ) calculated in aqueous solution. In line with experimental observations,  $\text{Ag}^+$  forms less stable coordination complexes compared to  $\text{Cu}^{2+}$ , with the metal located inside the macrocyclic cavity but weakly bound, as indicated by the coordination bond lengths exceeding 2.5 Å. This behavior is reflected in the Gibbs free energy value for the complex formation, which increases by approximately  $+10 \text{ kcal}\cdot\text{mol}^{-1}$  in presence of  $\text{Ag}^+$  rather than  $\text{Cu}^{2+}$  (**Table 3**). The two most stable configurations were identified, which have similar formation free energies, but different structural features (**Figure 8**).

The first one, denoted as  $[\text{Ag}^+-4\text{N}_{\text{cy}}1\text{N}_{\text{py}}1\text{S}]$ , has a Gibbs free energy of  $-21.7 \text{ kcal}\cdot\text{mol}^{-1}$  (**Table 3**) corresponding to a  $\log\beta$  of 15.9. In this species, the  $\text{Ag}^+$  ion is located inside the cyclen backbone and coordinates the four nitrogen atoms of the macrocycle, one pyridine nitrogen and one sulfur-containing side arm. The second configuration, named  $[\text{Ag}^+-4\text{N}_{\text{cy}}2\text{N}_{\text{py}}]$ , is slightly less stable and features the coordination of all nitrogen atoms of DO2S2Py to the metal. The calculated Gibbs free energy is  $-21.3 \text{ kcal}\cdot\text{mol}^{-1}$  (**Table 3**) corresponding to a  $\log\beta$  of 15.6. Both complexes are therefore predicted to be formed in aqueous solution, with  $\log\beta$  values close to the experimentally reported one of 16.94.

When both sulfur atoms, even if softer than nitrogen, are coordinated to  $\text{Ag}^+$ , a decrease in free energy and  $\log\beta$  is observed (**Figure S29**). For this configuration, named  $[\text{Ag}^+-4\text{N}_{\text{cy}}2\text{S}]$ , the Gibbs free energy is  $-17.5 \text{ kcal}\cdot\text{mol}^{-1}$  (**Table 3**) and the calculated  $\log\beta$  is 12.8.



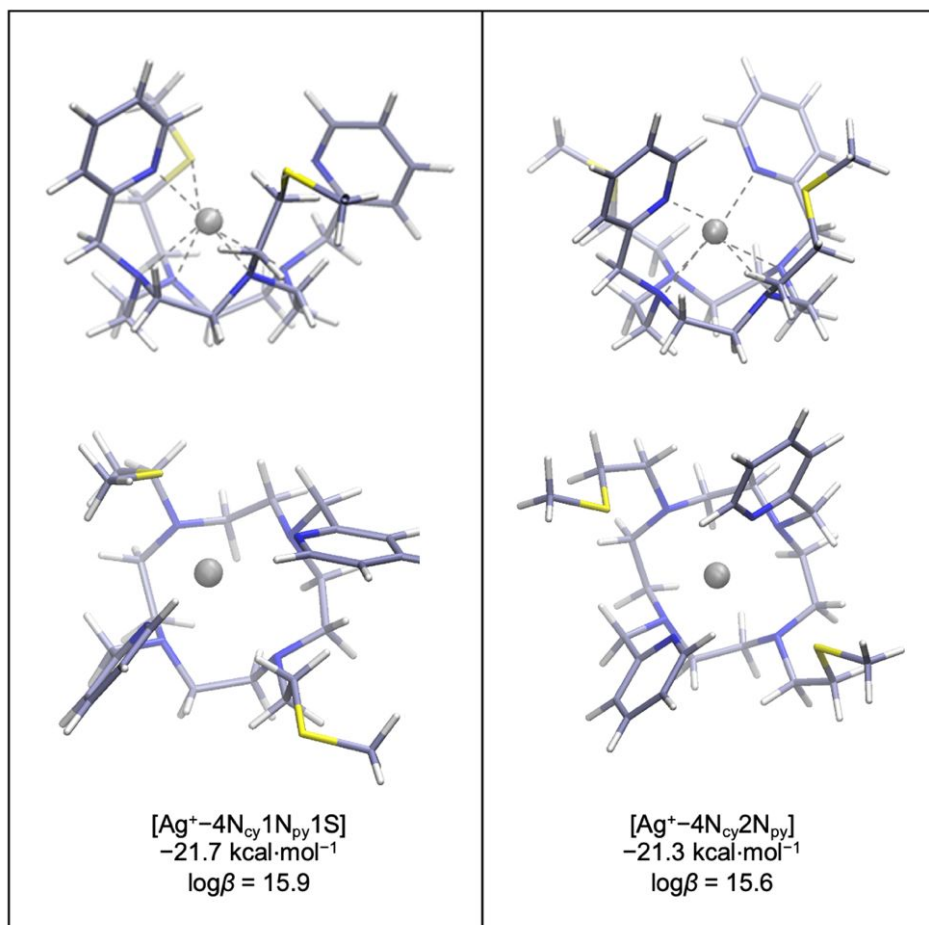


**Figure 8.** DFT optimized geometries of the most stable structures of  $[\text{Ag}(\text{DO2S2Py})]^+$  calculated in water together with the relative binding energies ( $\text{kcal}\cdot\text{mol}^{-1}$ ).

## 2.6 Dissociation Kinetics of DO2S2Py Complexes

The thermodynamic stability of a radiometal complex is a critical requirement for its use in radiopharmaceutical applications. However, once administered *in vivo*, the complex is exposed to a dynamic and competitive biological environment where various endogenous species may challenge the integrity of the complex. These non-equilibrium conditions may lead to demetallation events from the chelator, resulting in the release of the metal ion and its potential accumulation in non-target tissues. Consequently, different experiments were conducted to assess the kinetic inertness of the investigated  $\text{Cu}^{2+}$  and  $\text{Ag}^+$  complexes.

**2.6.1 Presence of Biologically Relevant Ions.** Challenge experiments were conducted using physiologically relevant cations ( $\text{Mg}^{2+}$ ,  $\text{Ca}^{2+}$  and  $\text{Zn}^{2+}$ ) as well as phosphate buffer (pH 7.4) to mimic the conditions of biological fluids.



Representative time-dependent UV-Vis spectra for  $[\text{Cu}(\text{DO2S2Py})]^{2+}$  in different competitive media are shown in **Figure S30**. Notably, no significant spectral changes were observed over 24 hours, indicating that  $[\text{Cu}(\text{DO2S2Py})]^{2+}$  is inert under these conditions and that DO2S2Py does not form stable complexes with the selected competing cations, as no spectral changes relative to the free ligand were observed upon addition of these ions. Furthermore, the complex remained stable in phosphate-buffered saline (PBS), further supporting its high kinetic robustness under physiological conditions. A similar behavior was observed for the  $\text{Ag}^+$  counterpart, as illustrated in **Figure S31**. No evidence of demetallation or complex degradation was detected over time, underscoring the exceptional inertness of this complex.

**2.6.2 Acidic Conditions.** The acid-induced decomplexation kinetics of  $[\text{Cu}(\text{DO2S2Py})]^{2+}$  and  $[\text{Ag}(\text{DO2S2Py})]^+$  were assessed by incubating the pre-formed complexes in strongly acidic media (pH  $\ll$  2). Although such extreme conditions are not physiologically relevant, this assay provides a stringent test of kinetic inertness and allows quantitative comparisons with other chelators under harsh conditions.

Representative changes in the electronic spectra of  $[\text{Cu}(\text{DO2S2Py})]^{2+}$  upon incubation in increasingly acidic solutions are shown in **Figure S32** and the corresponding dissociation half-lives ( ${}^d t_{1/2}$ ) are reported in **Table S6**. The observed first-order dissociation rate constants ( ${}^d k_{\text{obs}}$ ) exhibit a linear dependence on proton concentration (**Figure S33**), suggesting that only one complex undergoes dissociation and that the protonation constant of the predissociation step is low.<sup>40</sup> Accordingly, the second-order rate constant ( ${}^d k$ ) was derived using the relationship  ${}^d k_{\text{obs}} = {}^d k[\text{H}^+]$ .

A comparison with  ${}^d k$  values for other sulfur-containing chelators is provided in **Table 3**. Based on the data, the kinetic inertness of the  $\text{Cu}^{2+}$  complexes follows the order: DO2A2S > DO2S2Py  $\approx$  DO4S  $\gg$  TE4S. This indicates that the inclusion of both sulfur- and pyridine-containing pendant arms on a cyclen backbone does not enhance the kinetic inertness of the complex against acid-induced dissociation, which on the other hand is enhanced in the presence of negatively charged groups such as the acetate of DO2A2S. However, this ranking reflects behavior under highly acidic conditions and may not directly translate to *in vivo* environments, where such extreme acidity is not encountered. Therefore, other tests such as the human serum stability were conducted (see below).

**Table 3.** Comparison of the acid-assisted dissociation kinetic constant  ${}^d k$  of  $[\text{Cu}(\text{DO2S2Py})]^{2+}$  and  $\text{Cu}^{2+}$  complexes of other sulfur-containing chelators.<sup>40</sup>

	DO4S	DO2A2S	TE4S	DO2S2Py
${}^d k$ [ $\text{M}^{-1}\cdot\text{s}^{-1}$ ]	$(5.7 \pm 0.1) \cdot 10^{-4}$	$(1.04 \pm 0.02) \cdot 10^{-4}$	$\sim 10^{-2}$	$(5.32 \pm 0.05) \cdot 10^{-4}$



The decomplexation kinetics of the  $\text{Ag}^+$  counterpart were only qualitatively evaluated. Indeed, upon dissolution of  $[\text{AgDO2S2Py}]^+$  in highly acidic conditions ( $\text{pH} \ll 2$ ), the  $^1\text{H}$  NMR spectrum changes immediately, becoming identical to that of the free ligand with no further spectral changes over time. This observation suggests that the  $\text{Ag}^+$  complex is significantly more labile under these conditions than its  $\text{Cu}^{2+}$  counterpart. This difference likely arises from the intrinsic electronic characteristics of the two metals:  $\text{Ag}^+$  is a  $d^{10}$  ion, generally more labile, while  $\text{Cu}^{2+}$  is a  $d^9$  ion, forming more inert complexes.

**2.6.3. Copper reduction.** A potential decomplexation pathway for  $\text{Cu}^{2+}$  complexes *in vivo* involves the reduction of  $\text{Cu}^{2+}$  to  $\text{Cu}^+$  by endogenous bioreductants, followed by dissociation from the chelator and subsequent transchelation to endogenous  $\text{Cu}^+$ -binding proteins. To investigate the ability of DO2S2Py to bind  $\text{Cu}^+$ , DFT calculations were carried out. All the optimized geometries for the complexes formed by the  $\text{Cu}^+$  ion and DO2S2Py are reported in **Figure S34**, and the most relevant bond distances are summarized in **Table S4**.

The theoretical results indicate that DO2S2Py can coordinate the  $\text{Cu}^+$  center, but the resulting complexes are approximately  $10 \text{ kcal}\cdot\text{mol}^{-1}$  less stable than the corresponding  $\text{Cu}^{2+}$  complexes (**Table 3**). Several attempts were made to explore in detail all the possible coordination modes, but only three distinct configurations were identified. In all cases,  $\text{Cu}^+$  is located within the macrocyclic cavity. In the first geometry, designated as  $[\text{Cu}^+-3\text{N}_{\text{cy}}1\text{N}_{\text{py}}]$ , the copper center forms three coordination bonds with three nitrogen atoms of the macrocyclic ring and additionally coordinates one of the two pyridine donors. In the second geometry, identified as  $[\text{Cu}^+-3\text{N}_{\text{cy}}1\text{S}]$ , the coordination of the pyridine nitrogen is replaced by the sulfur atom from one pendant arm.

The calculated free energy for the former is  $-26.1 \text{ kcal}\cdot\text{mol}^{-1}$ , corresponding to  $\log\beta = 19.1$ , whereas for the latter the free energy is  $-24.2 \text{ kcal}\cdot\text{mol}^{-1}$  with  $\log\beta = 17.7$  (**Table 3**). In the third configuration, denoted as  $[\text{Cu}^+-4\text{N}_{\text{cy}}]$ , the  $\text{Cu}^+$  center coordinates all four donor atoms of the cyclen ring, but this arrangement is approximately  $3 \text{ kcal}\cdot\text{mol}^{-1}$  less stable than the most favorable geometry (**Table 3**). The corresponding free energy is  $-23.2 \text{ kcal}\cdot\text{mol}^{-1}$  (**Table 3**), corresponding to  $\log\beta = 17.0$ . The reduced stability of the  $\text{Cu}^+$  complexes compared to the  $\text{Cu}^{2+}$  analogues can be rationalized in terms of a reduced macrocyclic effect, a trend widely reported in the literature for this metal center.<sup>54</sup> Under these conditions,  $\text{Cu}^+$  preferentially adopts a coordination number of four, and realizing this geometry requires several structural adjustments within the chelator to maximize the metal-ligand interactions.

Cyclic voltammetry (CV) was performed, and the resulting voltammograms are shown in **Figure S35**. Unexpectedly, the voltammogram of  $[\text{Cu}(\text{DO2S2Py})]^{2+}$  displayed an irreversible reduction signal located at approximately  $-0.5 \text{ V}$ . In the reverse scan, the voltammogram instead shows a peak at around  $0.05 \text{ V}$ , very close to the oxidation peak of free  $\text{Cu}^+$  in solution.<sup>38</sup> This suggests that the ligand is unable to effectively stabilize the reduced  $\text{Cu}^+$  species.



This voltammetric behavior appears surprising given that DO2S2Py can bind  $\text{Ag}^+$  and that DFT calculations support the formation of stable complexes with  $\text{Cu}^+$  as well. We hypothesize that, upon reduction, the ligand cannot reorganize rapidly enough to enable an effective coordination by the softer sulfur donors, likely due to steric hindrance and the conformational rigidity imposed by the bulky pyridine groups. This behavior contrasts with that of other sulfur-containing chelators, such as DO2A2S and DO4S, which have been shown to stabilize both oxidation states of copper.<sup>38</sup> However, a similar lability is often observed in the literature with other cyclen-based chelators.<sup>50,51</sup>

## 2.7. Radiolabeling of DO2S2Py

**2.7.1.  $^{64}\text{Cu}$   $\text{Cu}^{2+}$ .** Concentration- ( $10^{-4} \text{ M} < C < 10^{-8} \text{ M}$ ), time- (5 min  $< t < 60$  min), pH- (4.5 and 7), and temperature-dependent (RT and  $95^\circ\text{C}$ ) radiolabeling experiments with  $^{64}\text{Cu}$   $\text{Cu}^{2+}$  were conducted. The results are summarized in **Figure 9**.

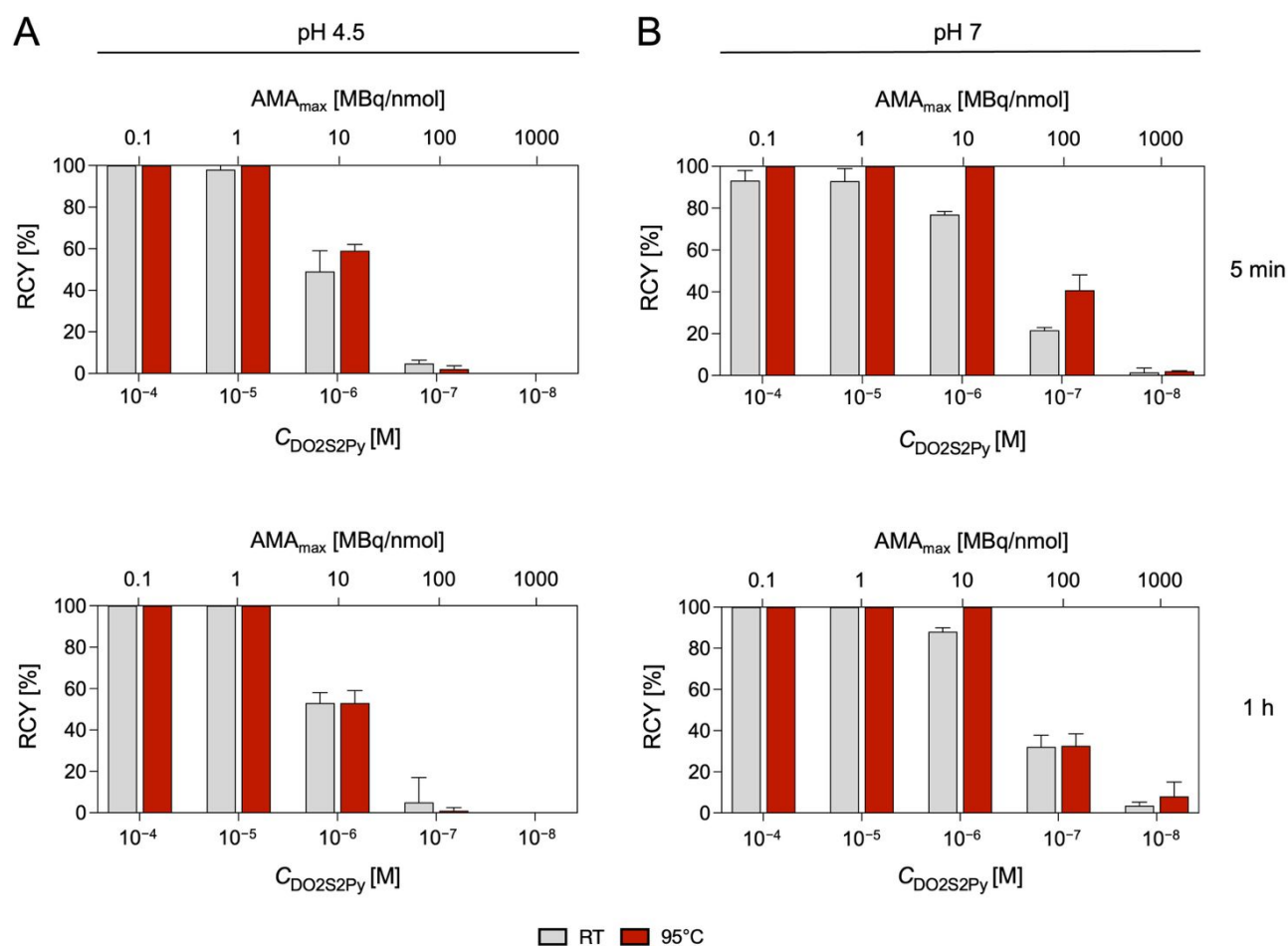


**Figure 9.** Concentration-, time-, and temperature-dependent  $^{64}\text{Cu}$   $\text{Cu}^{2+}$  radiolabeling with DO2S2Py at (A) pH 4.5 and (B) pH 7.



At pH 4.5, quantitative radiochemical yields (RCY > 99%) were obtained at a maximum apparent molar activity ( $AMA_{\max}$ ) of 1 MBq/nmol (corresponding to a  $C_{\text{DO2S2Py}} = 10^{-5}$  M) both at room temperature and 95°C. Notably, no significant differences in the achievable  $AMA_{\max}$  were observed upon extending the reaction time from 5 min to 60 min. Indeed, when the chelator concentration was reduced to  $10^{-6}$  M and  $10^{-7}$  M, the RCY dropped below 50% and 10%, respectively, highlighting a limit in the achievable apparent molar activity under these conditions.

At pH 7, quantitative RCY > 95% was achieved at room temperature within 5 min at  $AMA_{\max} = 1$  MBq/nmol ( $C_{\text{DO2S2Py}} = 10^{-5}$  M). Also in this case, prolonged incubation did not increase the  $AMA_{\max}$  that remained limited to 1 MBq/nmol. In contrast, heating the reaction mixture at 95°C enabled a tenfold increase in apparent molar activity ( $AMA_{\max} = 10$  MBq/nmol,  $C_{\text{DO2S2Py}} = 10^{-6}$  M) with respect to ambient temperature. No impact on the reaction time was observed.

The differences observed between the two investigated pH values are consistent with previous results obtained using analogous sulfur-rich chelators.<sup>39,41</sup> These changes are attributed to the lower degree of protonation of the chelator at higher pH, which facilitates complexation by reducing electrostatic repulsion between the protonated donor sites and the incoming  $[^{64}\text{Cu}]\text{Cu}^{2+}$  ions.

Compared to one of the current standards for radiocopper chelation, NOTA, DO2S2Py shows a similar performance at both pH values (**Figure S36**). In contrast, when evaluated against previously reported sulfur-rich cyclen-based chelators (e.g., DO4S and DO2A2S), DO2S2Py performs at a comparable or slightly lower level. However, this apparent discrepancy may arise from the use of different copper batches in the respective experiments.<sup>39</sup>

**2.7.2.  $[^{111}\text{Ag}]\text{Ag}^+$ .** Radiolabeling experiments were performed with  $[^{111}\text{Ag}]\text{Ag}^+$ , investigating the influence of chelator concentration ( $10^{-4}$  M <  $C$  <  $10^{-7}$  M), reaction time (5 min and 60 min), and temperature (RT and 95°C). Due to the limited availability of  $[^{111}\text{Ag}]\text{Ag}^+$ , only one pH condition (pH 7.4) was tested, selected on the basis of the reaction conditions optimized in our previous works.<sup>42,43</sup> The results are reported in **Figure 10**.

Quantitative radiometal incorporation was achieved up to 0.1 MBq/nmol within 5 min. The RCY dropped to approximately 50% at 100 MBq/nmol. Heating the reaction mixture to 95°C significantly enhanced the radiolabeling efficiency, increasing the  $AMA_{\max}$  to 1 MBq/nmol. Extending the reaction time did not produce appreciable improvement in the radiometal incorporation.

Under these conditions, the  $AMA_{\max}$  attained was 1 MBq/nmol, roughly one order of magnitude lower than that observed with  $[^{64}\text{Cu}]\text{Cu}^{2+}$ . However, this difference may reflect varying levels of metal impurities between the two radioisotopes, which can influence complexation behavior. Consequently, no definitive conclusions regarding chelator selectivity or preference can be drawn. Nonetheless, the results indicate



that the chelator exhibits strong affinity for both radiometals. Compared to DO4S, the performance of DO2S2Py appears slightly inferior (**Figure S37**).

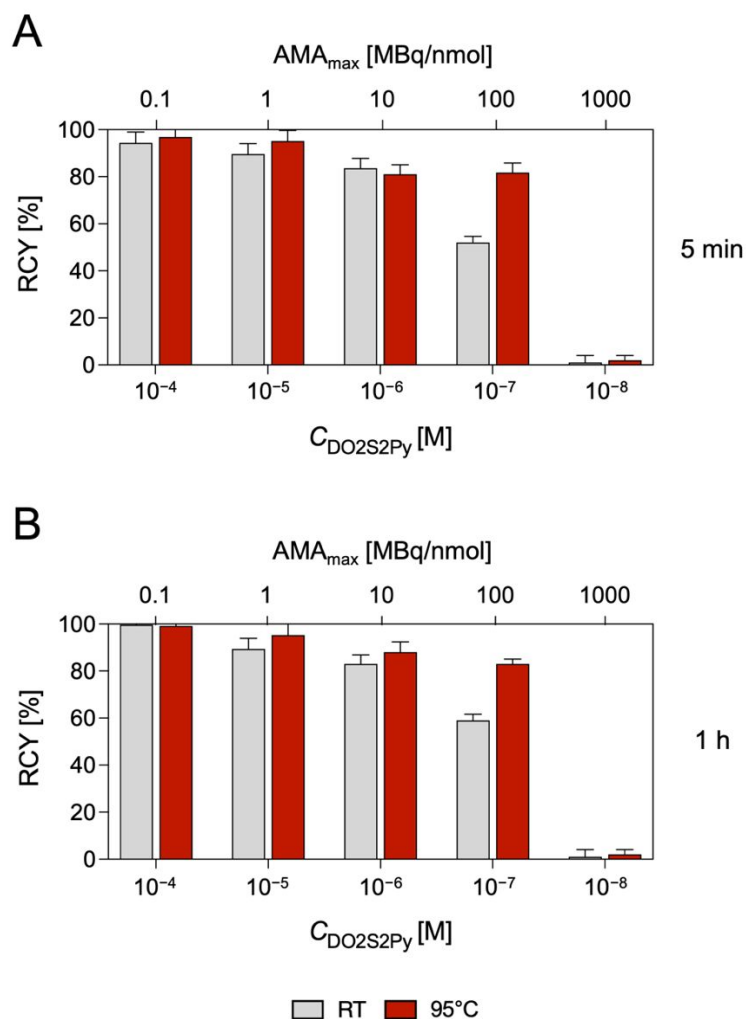


**Figure 10.** Concentration- and temperature-dependent  $[^{111}\text{Ag}]\text{Ag}^+$  radiolabeling with DO2S2Py at pH 7.4 after (A) 5 min and (B) 60 min.

### 2.8. *In Vitro* Stability in Biological Media of $[^{64}\text{Cu}][\text{Cu}(\text{DO2S2Py})]^{2+}$ and $[^{111}\text{Ag}][\text{Ag}(\text{DO2S2Py})]^+$

As the final step in evaluating DO2S2Py as a chelator for copper and silver radioisotopes, the *in vitro* stability of the corresponding radioactive complexes was assessed in PBS and human serum.

As illustrated in **Figure 11**,  $[^{64}\text{Cu}][\text{Cu}(\text{DO2S2Py})]^{2+}$  showed excellent stability under both conditions, with no detectable radiometal release and retention of > 95% integrity after 24 h.  $[^{111}\text{Ag}][\text{Ag}(\text{DO2S2Py})]^+$  displayed lower stability compared to its copper analogue: after 24 h, it maintained ~ 90% integrity in PBS, while it dropped to ~ 75% in human serum. The modest decomplexation observed in PBS likely



reflects competitions with chloride ions, while the further stability decline in serum is probably caused by interactions with serum components (e.g., albumin). However, it is important to note that  $[^{111}\text{Ag}][\text{Ag}(\text{DO2S2Py})]^+$  outperformed the previously best-performing chelator for silver radioisotopes (DO4S), underscoring the beneficial effect of incorporating pyridine arms (Figure S38). These additional donor groups appear to provide enhanced shielding of the metal center, thereby reducing susceptibility to competing biological ligands.

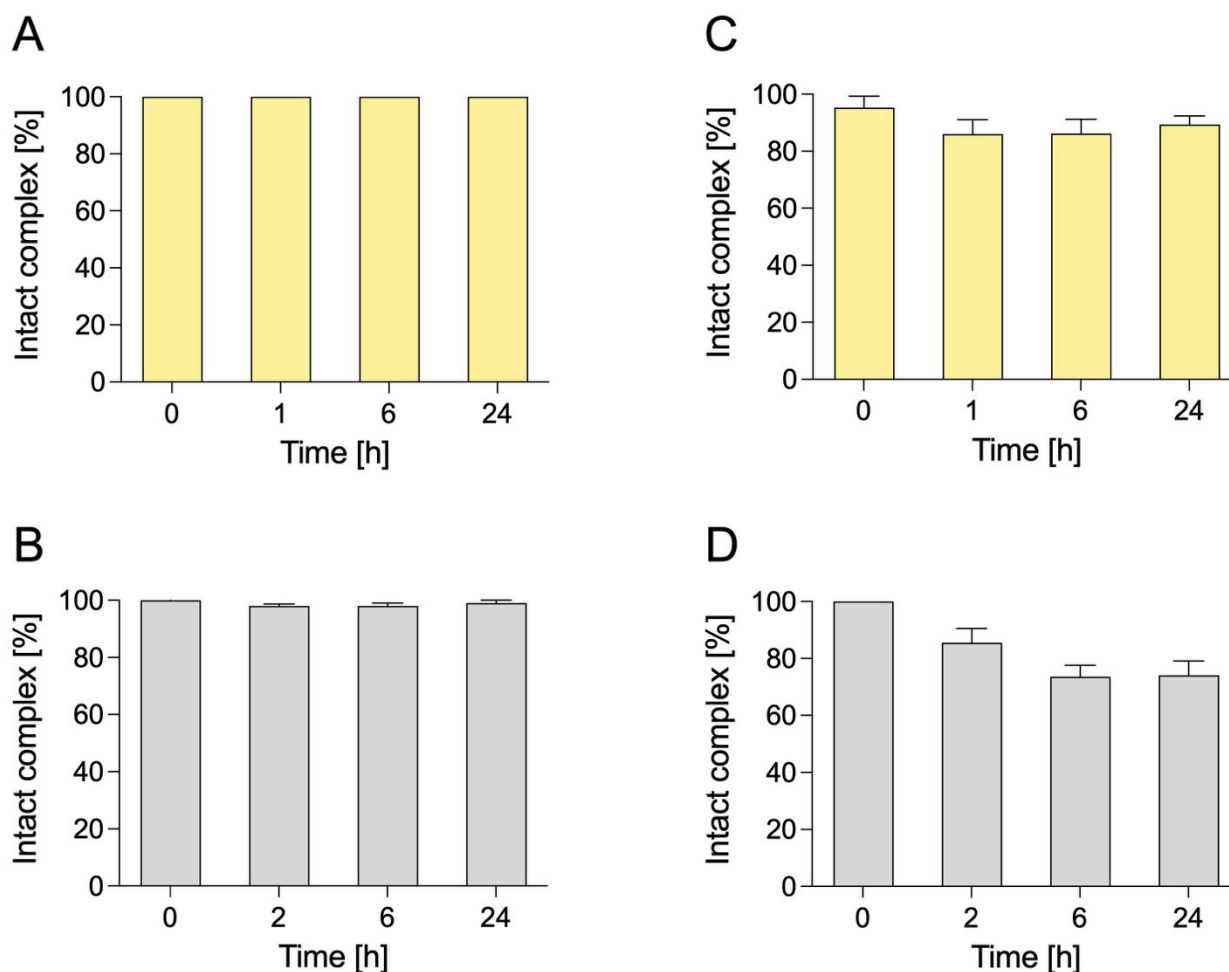


**Figure 11.** Integrity of (A, B)  $[^{64}\text{Cu}][\text{Cu}(\text{DO2S2Py})]^{2+}$  and (C, D)  $[^{111}\text{Ag}][\text{Ag}(\text{DO2S2Py})]^+$  in PBS (A and C) and human serum (B and D) (1:1 V/V dilution).



### 3. Experimental

#### 3.1. General

All solvents and reagents were purchased from commercial suppliers (Sigma-Aldrich, Aristar - VWR Chemicals, EMSURE, Merck, Chematech, Macrocyclics) and used without further purification. Ultrapure water (18.2 M $\Omega$ -cm) was obtained from a Milli-Q purification system and used throughout.

Organic reactions were monitored by thin-layer chromatography (TLC) on aluminum plates coated with silica gel 60 F<sub>254</sub> (Merck). Flash column chromatography was performed using high-purity silica gel (60 Å, 230-400 mesh, 40-63  $\mu$ m, Merck), with the appropriate eluents, as described in the corresponding section. The final product (DO2S2Py) was purified by reverse-phase semipreparative high-performance liquid chromatography (RP-HPLC) using a Phenomenex Luna C18 (150 mm  $\times$  100 mm) column. NMR spectra were recorded on a Bruker AVANCE AMX 400 spectrometer (<sup>1</sup>H: 400.12 MHz; <sup>13</sup>C: 100.13 MHz) or a Bruker AVANCE AMX 600 spectrometer equipped with a CryoProbe BBO H&F 5 mm in inverse detection (<sup>1</sup>H: 600.13 MHz, <sup>13</sup>C: 150.13 MHz). <sup>1</sup>H and <sup>13</sup>C{<sup>1</sup>H} NMR spectra are reported on the chemical shifts ( $\delta$ ) scale and referenced to residual solvent peaks or 3-(trimethylsilyl)propionic acid sodium salt (TSP) in D<sub>2</sub>O. Signal multiplicity is reported as follows: s = singlet, d = doublet, t = triplet, br = broad peak, m = multiplet. Mass spectrometry (MS) analyses were performed on an Agilent 6210 TOF LC/MS, an Advion expression LC-MS, or an Agilent 6300 Ion Trap LC-MS system equipped with an electrospray (ESI) source. The pH was measured with a Mettler Toledo SevenEasy pH-meter and a Crison (pH 0-14) combined glass electrode. UV-Vis spectra were recorded on a JASCO V-770 UV/vis/NIR spectrophotometer over the 200-800 nm spectral range, using quartz cells with 1 cm optical path. EPR spectra were acquired with a Bruker EleXsys E500 spectrometer. CV measurements were carried out using an Autolab PGSTAT-30 potentiostat, under the control of GPES software. Unless otherwise stated, no uncommon hazards were noted during the experiments.

#### 3.2 Synthesis

**1,7-Bis(tert-butyloxycarbonyl)-1,4,7,10-tetraazacyclododecane (di-Boc-cyclen).** Under Ar atmosphere, cyclen (400 mg, 2.32 mmol, 1.0 eq) was dissolved in dry methanol (20 mL). The solution was cooled in an ice bath, and N-Boc-succinimide (Boc-OSu, 1.00 g, 4.65 mmol, 2.0 eq), previously dissolved in methanol (2 mL), was added dropwise over 30 min. The reaction mixture was then allowed to warm to room temperature and stirred overnight. After completion, the solvent was removed under reduced pressure. The resulting residue was redissolved in 3 M NaOH and extracted with chloroform (3x). The combined organic layers were dried over anhydrous Na<sub>2</sub>SO<sub>4</sub>, filtered through a cotton plug, and concentrated under reduced pressure. The crude product was purified by flash column chromatography



on silica gel using a mixture of isopropanol and aqueous ammonia (8:2) as eluent to afford di-Boc-cyclen as a colorless oil (520.8 mg, yield = 60%).  $^1\text{H}$  NMR (400 MHz,  $\text{CDCl}_3$ ,  $25^\circ\text{C}$ )  $\delta$  (ppm): 3.26 (t, 8 H,  $\text{NCH}_2$ ), 3.03 (s, 2 H, NH), 2.76 (t, 8 H,  $\text{NCH}_2$ ), 1.37 (s, 18 H,  $\text{CH}_3$ ). ESI-MS:  $m/z$  373.28 (found); 373.28 (calc. for  $[\text{C}_{18}\text{H}_{37}\text{N}_4\text{O}_4]^+$ ).

**1,7-Bis(tert-butyloxycarbonyl)-4,10-bis(2-(methylsulfonyl)ethyl)-1,4,7,10 tetraazacyclododecane (di-Boc-DO2S).** Di-Boc-cyclen (447.0 mg, 1.2 mmol, 1 eq) was dissolved in dry acetonitrile (40 mL) under Ar atmosphere.  $\text{K}_2\text{CO}_3$  (1.79 g, 12.96 mmol, 8 eq) was added, followed by the addition of 2-chloroethylmethyl sulfide (641  $\mu\text{L}$ , 6.44 mmol, 4 eq). The reaction mixture was heated at  $50^\circ\text{C}$  for 2 days. After cooling to room temperature, the mixture was filtered through filter paper, and the solvent was removed under reduced pressure. The crude mixture was purified by flash column chromatography on silica gel using a gradient of dichloromethane/methanol (from 99:1 + 1%  $\text{NH}_3$  to 95:5 + 1%  $\text{NH}_3$ ). The desired product, di-Boc-DO2S, was obtained as a light-yellow oil (210.5 mg, 33 % yield).  $^1\text{H}$  NMR (400 MHz,  $\text{CDCl}_3$ ,  $25^\circ\text{C}$ )  $\delta$  (ppm): 3.34 (s, 8 H,  $\text{NCH}_2$ ), 2.67 (t, 12 H,  $\text{NCH}_2$ ), 2.54 (t, 4 H,  $\text{SCH}_2$ ), 2.09 (s, 6 H,  $\text{SCH}_3$ ), 1.43 (s, 18 H,  $\text{CH}_3$ ).  $^{13}\text{C}$  NMR (400 MHz,  $\text{CDCl}_3$ ,  $25^\circ\text{C}$ )  $\delta$  (ppm): 156.0 (C=O), 79.5 ( $-\underline{\text{C}}(\text{CH}_3)$ ), 54.3 + 54.7 ( $\text{NCH}_2$ ), 46.8 ( $\text{NCH}_2$ ), 31.5 ( $\text{SCH}_2$ ), 28.6 ( $\text{CH}_3$ ), 15.9 ( $\text{SCH}_3$ ). ESI-MS:  $m/z$  521.32 (found); 521.32 (calc. for  $[\text{C}_{24}\text{H}_{49}\text{N}_4\text{O}_4\text{S}_2]^+$ ).

**1,7-Bis(2-(methylsulfonyl)ethyl)-1,4,7,10-tetraazacyclododecane (DO2S).** Di-Boc-DO2S (150 mg) was dissolved in dichloromethane (9 mL), and trifluoroacetic acid (TFA, 10% in dichloromethane) was added dropwise (3 mL) at room temperature. The reaction mixture was stirred overnight. After completion, the solvent was removed under reduced pressure, and the residue was co-evaporated with toluene (3x) to remove residual TFA. The resulting crude was extracted with NaOH 20% and dichloromethane (3x). The combined organic layers were dried over anhydrous  $\text{Na}_2\text{SO}_4$ , filtered, and concentrated under reduced pressure to afford DO2S as a yellow oil (160 mg, quantitative yield).  $^1\text{H}$  NMR (400 MHz,  $\text{CDCl}_3$ ,  $25^\circ\text{C}$ )  $\delta$  (ppm): 2.60-2.55 (m, 24 H,  $\text{NCH}_2$  +  $\text{SCH}_2$ ), 2.05 (s, 6 H,  $\text{SCH}_3$ ).  $^{13}\text{C}$  NMR (400 MHz,  $\text{CDCl}_3$ ,  $25^\circ\text{C}$ )  $\delta$  (ppm): 53.8 ( $\text{NCH}_2$ ), 52.1 ( $\text{NCH}_2$ ), 45.3 ( $\text{NCH}_2$ ), 32.8 ( $\text{SCH}_2$ ), 15.7 ( $\text{SCH}_3$ ). ESI-MS:  $m/z$  321.21 (found); 321.21 (calc. for  $[\text{C}_{14}\text{H}_{33}\text{N}_4\text{S}_2]^+$ ).

**1,7-Bis(2-(methylsulfonyl)ethyl)-4,10-bis(pyridin-2-ylmethyl)-1,4,7,10-tetraazacyclododecane (DO2S2Py).** DO2S-2TFA (98.1 mg, 0.18 mmol, 1 eq) was dissolved in dry acetonitrile (10 mL) under Ar atmosphere.  $\text{K}_2\text{CO}_3$  (138 mg, 1 mmol, 5 eq) was added, followed by the dropwise addition of 2-(bromomethyl)pyridine hydrobromide (136 mg, 0.54 mmol, 3 eq) dissolved in acetonitrile (1 mL). The reaction mixture was stirred at room temperature for 3 days. The solvent was removed under reduced



pressure, and the crude product was purified by HPLC to afford DO2S2Py as a yellow oil (34.8 mg, yield 38%).  $^1\text{H}$  NMR (400 MHz,  $\text{D}_2\text{O}$ ,  $25^\circ\text{C}$ )  $\delta$  (ppm): 8.51 (d, 2 H,  $\text{H}_{\text{Py}}$ ), 7.89 (t, 2 H,  $\text{H}_{\text{Py}}$ ), 7.49 (d, 2 H,  $\text{H}_{\text{Py}}$ ), 7.41 (t, 2 H,  $\text{H}_{\text{Py}}$ ), 3.81 (s br, 4 H,  $\text{NCH}_2$ ), 2.93 (s br, 8 H,  $\text{NCH}_2$ ) + 2.76 (s br, 12 H,  $\text{NCH}_2$ ), 2.55 (t, 4 H,  $\text{SCH}_2$ ), 1.97 (s, 6 H,  $\text{SCH}_3$ ).  $^{13}\text{C}$  NMR (400 MHz,  $\text{D}_2\text{O}$ ,  $25^\circ\text{C}$ )  $\delta$  (ppm): 171.1 ( $\text{C}_{\text{py}}$ ), 148.6 ( $\text{C}_{\text{py}}$ ), 138.3 ( $\text{C}_{\text{py}}$ ), 125.1 ( $\text{C}_{\text{py}}$ ), 123.7 ( $\text{C}_{\text{py}}$ ), 60.0 ( $\text{NCH}_2$ ), 51.3 + 48.3 ( $\text{NCH}_2$ ), 26.4 ( $\text{SCH}_2$ ), 14.5 ( $\text{SCH}_3$ ). ESI-MS:  $m/z$  503.26 (found); 503.30 (calc. for  $[\text{C}_{26}\text{H}_{43}\text{N}_6\text{S}_2]^+$ ).

### 3.3 Coordination Chemistry

#### 3.3.1 General

Stock solutions of DO2S2Py were prepared by dissolving a weighed amount of ligand directly in Milli-Q water to achieve a concentration of approximately  $2 \cdot 10^{-3}$  M.  $\text{Cu}^{2+}$  and  $\text{Ag}^+$  stock solutions were prepared from analytical-grade salt ( $\text{CuCl}_2$  or  $\text{AgNO}_3$ ) and standardized using ICP-MS ( $10^{-3}$ - $10^{-2}$  M). The ionic strength ( $I$ ) was maintained at 0.15 M using sodium chloride ( $\text{NaCl}$ ) or sodium nitrate ( $\text{NaNO}_3$ ), as specified in each case. All experiments were performed in MilliQ water at least in triplicate to ensure reproducibility.

#### 3.3.2 Formation Kinetics

The complexation kinetics were qualitatively assessed at ambient temperature by recording the UV-Vis ( $\text{Cu}^{2+}$ ) or  $^1\text{H}$ -NMR ( $\text{Ag}^+$ ) spectra of aqueous solutions containing the metal ion and DO2S2Py immediately after the mixing and over time. These solutions were prepared at a final concentration equal to  $10^{-3}$  M for  $^1\text{H}$  NMR and  $10^{-3}$ - $10^{-4}$  M for UV-Vis (1:1 metal-to-ligand ratio) in buffered media (e.g., pH 2 HCl  $10^{-2}$  M, pH 4.5 acetic/acetate buffer). To ensure the equilibrium was reached, the spectra of all samples were also re-acquired after heating at  $T = 80^\circ\text{C}$  until no further changes were observed.

#### 3.3.3 Thermodynamic Measurements

**Potentiometry.** Automatic pH-potentiometric titrations of DO2S2Py,  $\text{Cu}^{2+}$ -DO2S2Py, and  $\text{Ag}^+$ -DO2S2Py were carried out as described in detail in previous works.<sup>38,40-42</sup>

**NMR.** Variable-pH  $^1\text{H}$  NMR spectra of DO2S2Py ( $\sim 10^{-3}$  M) or  $\text{Ag}^+$ -DO2S2Py ( $\sim 10^{-3}$  M,  $\text{Ag}^+:\text{L}$  molar ratio of 1:1) were recorded at  $T = 25^\circ\text{C}$  in  $\text{D}_2\text{O}$ . The pH was adjusted by proper additions of  $\text{DNO}_3/\text{DCI}$  or  $\text{CO}_2$ -free  $\text{NaOD}$ . 0.41 log units were added to the instrumental pH values to account for isotopic effects, i.e. pD values instead of pH ones were considered..



**UV-Vis.** Variable-pH UV-Vis spectrophotometric titrations were conducted using the in-cell method for both the free DO2S2Py ( $C_L = 10^{-3} - 10^{-2}$  M) and Cu<sup>2+</sup>-DO2S2Py mixture ( $C_{Cu} = C_L = 10^{-3} - 10^{-2}$  M, pH > 2) at  $T = 25^\circ\text{C}$  and  $I = 0.15$  M NaCl. At pH < 2, the out-of-cell method was employed for Cu<sup>2+</sup>-DO2S2Py, as described in our previous works.<sup>40,41,55</sup> Small volumes (~  $\mu\text{L}$  range) of HCl and/or NaOH were used to adjust the pH. The electronic spectra were recorded, and the equilibrium was reached when no further changes in either the pH or the electronic spectra were observed.

**Data Treatment.** The protonation constants ( $pK_a$ ) and overall equilibrium constants ( $\log\beta$ ) were obtained by refinement of the thermodynamic data using different software (PITMAP, HypNMR, HyperSpec), as described in our previous publications.<sup>41,55–57</sup> Hydrolysis constants and solubility products of Cu<sup>2+</sup> and Ag<sup>+</sup> in aqueous ionic media were taken from the literature.<sup>58</sup>

**EPR measurements.** EPR spectra were recorded with a BRUKER EleXsys E500 spectrometer using microwave frequency equal to 9.54 GHz, 13 mW microwave power, 5 G modulation amplitude and 100 kHz modulation frequency. Cu<sup>2+</sup>-DO2S2Py aqueous solutions were prepared ( $10^{-3}$  M) and NaOH and HCl solutions were used to set the pH. The room temperature EPR spectra were recorded in capillaries (6 scans). For the frozen solution spectra 0.2 mL samples were diluted with 0.05 mL of methanol to avoid crystallization of water and transferred into EPR tubes. Anisotropic EPR spectra were recorded in a dewar containing liquid nitrogen (77 K). The spectra were simulated by the “ep<sup>r</sup>” program<sup>59</sup> using axial  $g$ -tensor ( $g_{\perp}$ ,  $g_{\parallel}$ ) and copper hyperfine tensor ( $A_{\perp}^{\text{Cu}}$ ,  $A_{\parallel}^{\text{Cu}}$ ) values. Orientation dependent linewidth parameters ( $\alpha$ ,  $\beta$ ,  $\gamma$ ) were used to fit the linewidths through the equation  $\sigma_{M_l} = \alpha + \beta M_l + \gamma M_l^2$ , where  $M_l$  denotes the magnetic quantum number of Cu<sup>2+</sup>. Since a natural CuCl<sub>2</sub> was used for the measurements, the spectra were calculated by the summation of spectra of <sup>63</sup>Cu and <sup>65</sup>Cu weighted by their natural abundances. The room temperature spectra were simulated with the same software using the obtained anisotropic EPR parameters and fitting the rotational correlation times averaging the orientation dependence of the parameters.

### 3.5 Computational Details

All the molecular geometry optimizations were performed by using the Gaussian16 package.<sup>60</sup> DFT level of theory was employed adopting the B3PW91 functional.<sup>61</sup> The 6-31G\* basis set was chosen for all the atoms except for the Ag and Cu atoms for which the LANL2DZ pseudo-potential was employed together with the associated valence basis set.<sup>62</sup> A benchmark was carried out for selecting the most appropriate computational protocol able to reproduce the optical absorption spectra of the investigated systems simulated using time-dependent density functional theory (TDDFT) based on the optimized ground-state geometries. As a result of such benchmark for the Cu<sup>2+</sup> complexes, the 6-31G\* basis set adopted also



for the Cu center was identified as the best performing one. Frequency calculations were performed at the same level of theory for all the optimized geometrical structures to confirm their nature of minima and for zero-point energy correction calculations. All calculations were carried out in water solvent ( $\epsilon = 78.4$ ), using Tomasi's implicit polarizable continuum model (PCM) as implemented in Gaussian16.<sup>62–64</sup>

For each complexation reaction, the free energy was computed replacing water molecules in the reference complexes. The reference complex for  $\text{Cu}^{2+}$  is square planar, with four water molecules in the first coordination sphere and two water molecules in the second coordination sphere. For  $\text{Ag}^+$ , the reference complex is linear, with two water molecules in the first coordination sphere.

The free energies of formation of these complexes are calculated using the reaction (1):



where L represents DO2S2Py,  $n$  corresponds to the number of coordinated water molecules in the reference complex (6 for  $\text{Cu}^{2+}$ , representing the hexa-aquo complex, and 2 for  $\text{Ag}^+$ , representing the bi-aquo complex), and  $z$  denotes the overall charge of the complex (+2 for  $\text{Cu}^{2+}$  and +1 for  $\text{Ag}^+$ ).

Gibbs free energies were obtained at  $T = 25^\circ\text{C}$  and 1 atm including zero-point and thermal corrections. Therefore, the formation energies of the examined complexes were calculated as:

$$\Delta G = \Delta G([\text{ML}]^z) + (n) \Delta G(\text{H}_2\text{O}) - \Delta G([\text{M}(\text{H}_2\text{O})_n]^z) - \Delta G(\text{L}) \quad (2)$$

The stability constant ( $\log\beta$ ) value is related to free energy change for the complexation reaction by:

$$\log\beta = -\frac{\Delta G}{2.303RT} \quad (3)$$

Complexation energies were corrected for the basis set superposition error (BSSE) by using the Boys-Bernardi counterpoise technique.<sup>65</sup>

### 3.6 Kinetic Inertness

**3.6.1 Competition with Metal Ions.** Competitive metal ions ( $\text{Zn}^{2+}$ ,  $\text{Mg}^{2+}$ ,  $\text{Ca}^{2+}$ ,  $n_{\text{competitor}}/n_{\text{complex}} = 10$ ) or PBS (1:1 V/V dilution) were added to a solution of the preformed complexes and spectral variations induced by the additions of the competitor were monitored at room temperature over time using UV-Vis ( $\text{Cu}^{2+}$ ;  $C_{\text{DO2S2Py}} = C_{\text{Cu}} = 1 \cdot 10^{-4}$  M) or  $^1\text{H-NMR}$  ( $\text{Ag}^+$ ;  $C_{\text{DO2S2Py}} = C_{\text{Ag}} = 1 \cdot 10^{-3}$  M). All experiments were performed in MilliQ water at least in triplicate to ensure reproducibility.



**3.6.2 Acid-Mediated Decomplexation Kinetics.** Acid-mediated decomplexation studies of  $[\text{Cu}(\text{DO2S2Py})]^{2+}$  were performed under pseudo-first-order conditions in HCl at  $T = 25^\circ\text{C}$ , as described in our previous work.<sup>40</sup> The  $^d k_{\text{obs}}$  values were calculated from the experimental data by using a single-exponential model  $A(t) = A(0) \cdot e^{-k_{\text{obs}} t}$ . The corresponding half-life was obtained from the equation  $t_{1/2} = \ln 2 / ^d k_{\text{obs}}$ .

### 3.7 Cyclic Voltammetry

CV measurements were carried out in a conventional three-electrode cell equipped with a glassy carbon (GC, Metrohm) working electrode, a platinum wire counter electrode, and an Ag/AgCl (3 M KCl, Amel) reference electrode. Prior to each experiment, the GC electrode was polished with 0.05  $\mu\text{m}$  alumina slurry and thoroughly rinsed with an ethanol/water mixture. Cyclic voltammograms were recorded at room temperature in aqueous 0.15 M  $\text{NaNO}_3$  containing  $\text{Cu}^{2+}$  ( $C_{\text{DO2S2Py}} = 8 \cdot 10^{-4}$  M) and ligand ( $C_{\text{Cu}} = 8 \cdot 10^{-4}$  M) at pH 7.

### 3.8 Radiochemical Experiments

*Caution!  $^{64}\text{Cu}$  and  $^{111}\text{Ag}$  are radionuclides that emit ionizing radiation and were manipulated in a specifically designed facility under appropriate safety controls.*

**3.8.1.  $^{64}\text{Cu}[\text{Cu}]^{2+}$ .**  $^{64}\text{Cu}[\text{Cu}]\text{Cl}_2$  was obtained as previously described and appropriately diluted in 0.05 M HCl.<sup>66</sup> DO2S2Py and NOTA (reference) stock solutions were prepared in ultrapure metal-free water at  $10^{-3}$  and diluted appropriately to give a serial dilution series ( $10^{-4}$ – $10^{-7}$  M). Radiolabeling was performed by mixing  $^{64}\text{Cu}[\text{Cu}]^{2+}$  (1 MBq, 10  $\mu\text{L}$ ) to a solution containing the ligand (10  $\mu\text{L}$ ) diluted in an appropriate buffer (80  $\mu\text{L}$  of either 0.1 M sodium acetate – final pH 4.5, or PBS 1x – final pH 7). A negative control (free  $^{64}\text{Cu}[\text{Cu}]^{2+}$ ) was performed by substituting the ligand with an equal volume (10  $\mu\text{L}$ ) of  $\text{H}_2\text{O}$ . Different apparent molar activities were tested from 0.1 to 1000 MBq/nmol, corresponding to a final ligand concentration ranging from  $10^{-4}$  to  $10^{-8}$  M. The reaction mixtures were allowed to react at ambient temperature or  $95^\circ\text{C}$  and the radiochemical yields (RCY%) were monitored at different time points (5 min – 1 h). All radiolabeling reactions were repeated at least in triplicate. RCY% was determined via radio-thin layer chromatography (radio-TLC) using iTLC-SA plates as stationary phase and EDTA (0.1 M, pH 5) as mobile phase. Under these conditions, free  $^{64}\text{Cu}[\text{Cu}]^{2+}$  migrates with the solvent front ( $R_f = 1$ ) while  $^{64}\text{Cu}[\text{Cu}]^{2+}$  complexes remain at the baseline ( $R_f = 0$ ). The iTLC plates were analyzed on an Eckert & Ziegler AR-2000 TLC scanner, and all the data were processed with Eckert & Ziegler WinScan software.



**3.8.2. [ $^{111}\text{Ag}]\text{Ag}^+$ .**  $^{111}\text{Ag}$  was produced at the Institute Laue-Langevin (ILL, Grenoble, France) and purified at the Hevesy Laboratory (Denmark) using the anion exchange Dowex 1x8 and obtained in 6 M HCl. The fractions containing  $^{111}\text{Ag}$  were evaporated and subsequently diluted in 1 M HCl.<sup>43</sup> DO2S2Py and DO4S (reference) stock solutions were prepared in ultrapure metal-free water at  $10^{-3}$  M and diluted appropriately to give a serial dilution series ( $10^{-4}$ – $10^{-7}$  M). Radiolabeling was executed by the addition of [ $^{111}\text{Ag}]\text{Ag}^+$  (6.4  $\mu\text{L}$ , 1 MBq) to a solution containing the ligand (10  $\mu\text{L}$ ) at the proper concentration diluted in phosphate buffer (50 mM, pH 7.4, 83.6  $\mu\text{L}$ ). A negative control (free [ $^{111}\text{Ag}]\text{Ag}^+$ ) was performed by substituting the ligand with an equal volume of  $\text{H}_2\text{O}$ . Different apparent molar activities were tested from 0.1 to 1000 MBq/nmol, corresponding to a final ligand concentration ranging from  $10^{-4}$  to  $10^{-8}$  M. The radiolabeling reactions were conducted at RT or at  $T = 95^\circ\text{C}$ . All experiments were repeated in triplicate and monitored over time (5 min, 1 h) *via* radio-TLC using silica gel 60 F254 aluminum plates and  $\text{CHCl}_3:\text{CH}_3\text{OH}$  9:1 + 0.1%  $\text{NH}_4\text{OH}$  as mobile phase. Under these conditions, free [ $^{111}\text{Ag}]\text{Ag}^+$  is retained at the origin ( $R_f = 0$ ) while [ $^{111}\text{Ag}][\text{Ag}(\text{DO2S2Py})]^+$  has  $R_f = 0.6$ . To track the radiolabeling of [ $^{111}\text{Ag}][\text{Ag}(\text{DO4S})]^+$ , the conditions previously described were used.<sup>43</sup> The TLC plates were exposed to a multi-sensitive medium phosphor screen (Perkin Elmer) and analyzed using a Cyclone Plus Storage Phosphor System (Perkin Elmer).

### 3.8.3. *In Vitro* Stability Assays

The integrity of [ $^{64}\text{Cu}][\text{Cu}(\text{DO2S2Py})]^{2+}$  and [ $^{111}\text{Ag}][\text{Ag}(\text{DO2S2Py})]^+$  was assessed in PBS and human serum by diluting the radiolabeled complexes ( $\text{RCY} > 99\%$  prior to incubation) with an equal volume of PBS or human serum (1:1 V/V dilution), respectively. The 1:1 V/V dilution was selected to maintain consistency with previously conducted studies, allowing reliable comparison of the data. The solutions were incubated at  $T = 37^\circ\text{C}$  to simulate the biological environment. The integrity of the radiometal complexes was monitored over time *via* radio-TLC, using the mobile and stationary phases described above. Free [ $^{64}\text{Cu}]\text{Cu}^{2+}$  and free [ $^{111}\text{Ag}]\text{Ag}^+$  in human serum were used as controls. Any [ $^{64}\text{Cu}]\text{Cu}^{2+}$  that had transchelated with serum proteins migrated with EDTA solvent front ( $R_f \sim 1$ ), while intact radiometal complex remained at the baseline ( $R_f \sim 0$ ). In contrast, any [ $^{111}\text{Ag}]\text{Ag}^+$  that had transchelated with serum proteins remained at the baseline ( $R_f \sim 0$ ) while intact metal complex had  $R_f = 0.6$ . The percentage of intact complex was determined by integrating the areas under the curves corresponding to the free and intact species.



## 4. Conclusions

Coinage radiometals such as  $^{103/111}\text{Ag}$  and  $^{64/67}\text{Cu}$  offer significant opportunities for cancer theranostics by providing matched diagnostic and therapeutic radionuclides within the same chemical family. Their successful *in vivo* application, however, critically depends on chelators capable of maintaining stable metal coordination *in vivo*. Despite their promise, the clinical translation of  $^{103/111}\text{Ag}$  remains severely limited by the lack of robust chelating systems, while redox-induced decomplexation continues to challenge the stability of  $^{64/67}\text{Cu}$ -based radiopharmaceuticals. In this context, the development of a single ligand platform capable of efficiently coordinating both silver and copper represents a significant breakthrough that would enable the preparation of chemically analogous radiopharmaceuticals that differ only in radionuclide identity.

Building on our previous work on sulfur-containing macrocycles for the chelation of theranostic radiometals, we sought to enhance the biological stability of the resulting radiometal complexes. Although these earlier ligands displayed promising coordination properties, the corresponding radioactive complexes showed only moderate stability under biologically relevant conditions. To address this limitation, we incorporated pyridine donor units in the macrocyclic framework, creating a sterically protected coordination environment.

The resulting ligand, DO2S2Py, rapidly coordinates both  $\text{Cu}^{2+}$  and  $\text{Ag}^+$ , forming complexes that are highly thermodynamically stable and kinetically inert. In  $[\text{Cu}(\text{DO2S2Py})]^{2+}$ , the copper center adopts a distorted elongated octahedral geometry involving the two pyridine nitrogen atoms and the four nitrogens from the cyclen backbone ( $4\text{N}_{\text{cy}}2\text{N}_{\text{py}}$ ). In contrast,  $[\text{Ag}(\text{DO2S2Py})]^+$  displays multiple coordination modes in aqueous solutions ( $4\text{N}_{\text{cy}}1\text{N}_{\text{py}}1\text{S}$  and  $4\text{N}_{\text{cy}}2\text{N}_{\text{py}}$ ) reflecting the adaptable yet strongly binding nature of the ligand scaffold. In both cases, the pyridine donors play a key role in reinforcing metal coordination and enhancing complex stability.

Importantly, DO2S2Py also efficiently complexes the corresponding radioactive isotopes ( $^{64}\text{Cu}$  and  $^{111}\text{Ag}$ ) under highly diluted radiochemical conditions and mild labeling protocols.  $^{64}\text{Cu}$   $[\text{Cu}(\text{DO2S2Py})]^{2+}$  exhibited exceptional stability in biologically relevant media (> 95% intact after 24 h), specifically PBS and human serum. Although  $^{111}\text{Ag}$   $[\text{Ag}(\text{DO2S2Py})]^+$  was less stable (75% intact after 24 h in human serum), it showed improved performance compared to the current best-performing chelator for  $^{111}\text{Ag}$ , *i.e.* DO4S.

Collectively, these results demonstrate that incorporation of pyridine donors effectively enhances complex stability and inertness in biological environments, thereby validating our design strategy. Overall, DO2S2Py represents a significant step toward the development of a unified chelator platform capable of stabilizing theranostic coinage radiometals under physiologically relevant conditions.



**Author Contributions.** The manuscript was written through contributions of all authors. All authors have given approval to the final version of the manuscript. M.T. Conceptualization, Data curation, Formal Analysis, Investigation, Methodology, Project administration, Writing - original draft; F.P. Investigation, Methodology, Writing - review & editing; S.F. Methodology, Writing - review & editing; N.V.M. Investigation, Methodology, Writing - review & editing; M.J. Funding acquisition, Supervision, Resources, Writing - review & editing; H.M. Funding acquisition, Supervision, Writing - review & editing; V.D.M. Supervision, Writing - review & editing; L.P. Supervision, Resources, Writing - review & editing; E.F. Funding acquisition, Supervision, Resources, Writing - review & editing; E.S. Funding acquisition, Supervision, Resources, Writing - review & editing; M.A. Funding acquisition, Supervision, Writing - review & editing; C.F. Funding acquisition, Supervision, Resources, Writing - review & editing.

**Conflict of Interests.** The authors have no competing interests to declare.

**Data Availability.** The authors confirm that the data supporting the findings of this study are available within the article and its supplementary information (SI). SI content: NMR and MS characterization of di-Boc-cyclen, di-Boc-DO2S, DO2S, and DO2S2Py; pH-dependent  $^1\text{H}$  NMR and UV-Vis titrations of DO2S2Py and corresponding speciation plots; UV-Vis studies of  $\text{Cu}^{2+}$ -DO2S2Py (formation kinetics and thermodynamics); NMR characterization of  $\text{Ag}^+$ -DO2S2Py (formation kinetics and thermodynamics); ESI-MS analysis of  $\text{Cu}^{2+}$ -DO2S2Py; comparison of  $\text{pCu}^{2+}$  values with related py-containing chelators; EPR spectra of  $[\text{Cu}(\text{DO2S2Py})]^{2+}$ ; DFT data for  $\text{Cu}^{2+}$ -DO2S2Py,  $\text{Ag}^+$ -DO2S2Py, and  $\text{Cu}^+$ -DO2S2Py; kinetic studies in the presence of competing metal ions and PBS; acid-assisted decomplexation kinetics; cyclic voltammogram of  $[\text{Cu}(\text{DO2S2Py})]^{2+}$ ; radiochemistry studies with  $^{64}\text{Cu}$  and  $^{111}\text{Ag}$  and comparison with reference chelators (NOTA and DO4S).

**Acknowledgments.** This research was supported by the European Union's Horizon 2020 research and innovation program as a user project of PRISMAP – The European medical radionuclides program (GA 101008571) and the New Frontiers in Research Fund Transformation Program “Rare Isotopes to Transform Cancer Therapy” (NFRFT-2022-00269). TRIUMF receives funding from a contribution agreement with the National Research Council of Canada. The work was also partly supported by the Italian Ministry of Health - Ricerca Corrente Annual Program 2025, AUSL-IRCCS Reggio Emilia (Italy). The authors gratefully acknowledge Prof. Ulli Köster and ILL (Grenoble, France) for performing irradiations of  $^{110}\text{Pd}$  targets for PRISMAP. The authors would like to thank the “Centro Interdipartimentale Grandi Strumenti C.I.G.S.” of the University of Modena and Reggio Emilia (<https://www.cigs.unimore.it>, Modena, Italy) for NMR, mass spectrometers and their technical support.



## References

- 1 M. Tosato and M. Asti, Lights and Shadows on the Sourcing of Silver Radioisotopes for Targeted Imaging and Therapy of Cancer: Production Routes and Separation Methods, *Pharmaceuticals*, 2023, **16**, 929.
- 2 K. A. Morgan, S. E. Rudd, A. Noor and P. S. Donnelly, Theranostic Nuclear Medicine with Gallium-68, Lutetium-177, Copper-64/67, Actinium-225, and Lead-212/203 Radionuclides, *Chem. Rev.*, 2023, **123**, 12004–12035.
- 3 N. Yang, X. Guo, J. Ding, F. Wang, T. Liu, H. Zhu and Z. Yang, Copper-64 Based PET-Radiopharmaceuticals: Ways to Clinical Translational, *Semin. Nucl. Med.*, 2024, **54**, 792–800.
- 4 *Copper-64 Radiopharmaceuticals: Production, Quality Control and Clinical Applications*, International Atomic Energy Agency, Vienna, 2022.
- 5 <https://www-nds.iaea.org/relnsd/vcharthtml/VChartHTML.html> (accessed April 20 2026)
- 6 O. O. Krasnovskaya, D. Abramchuck, A. Erofeev, P. Gorelkin, A. Kuznetsov, A. Shemukhin and E. K. Beloglazkina, Recent Advances in  $^{64}\text{Cu}/^{67}\text{Cu}$ -Based Radiopharmaceuticals, *Int. J. Mol. Sci.*, 2023, **24**, 9154.
- 7 P. Kręćisz, K. Stefańska, J. Studziński, M. Pitucha, A. Czyłkowska and P. Szymański, Radiocopper in Radiopharmacy and Medical Use: Current Status and Perspective, *J. Med. Chem.*, 2025, **68**, 2356–2376.
- 8 E. Boros and A. B. Packard, Radioactive Transition Metals for Imaging and Therapy, *Chem. Rev.*, 2019, **119**, 870–901.
- 9 M. Shokeen and C. J. Anderson, Coordination Chemistry of Bifunctional Chemical Agents Designed for Applications in  $^{64}\text{Cu}$  PET Imaging for Alzheimer's Disease, *Acc. Chem. Res.*, 2009, **42**, 832–841.
- 10 P. J. Blower, J. S. Lewis and J. Zweit, Copper Radionuclides and Radiopharmaceuticals in Nuclear Medicine, *Nucl. Med. Biol.*, 1996, **23**, 957–980.
- 11 T. Mastren, V. Radchenko, J. W. Engle, J. W. Weidner, A. Owens, L. E. Wyant, R. Copping, M. Brugh, F. M. Nortier, E. R. Birnbaum, K. D. John and M. E. Fassbender, Chromatographic Separation of the Theranostic Radionuclide  $^{111}\text{Ag}$  From a Proton Irradiated Thorium Matrix, *Anal. Chim. Acta*, 2018, **998**, 75–82.
- 12 M. Tosato, A. Gandini, S. Happel, M. Bas, A. Donzella, A. Zenoni, A. Salvini, A. Andrighetto, V. Di Marco and M. Asti, Chromatographic Separation of Silver-111 from Neutron-irradiated Palladium Target: Toward Direct Labeling of Radiotracers, *EJNMMI Radiopharm. Chem.*, 2023, **8**, 43.
- 13 T. A. Aweda, O. Ikotun, T. Mastren, C. L. Cannon, B. Wright, W. J. Youngs, C. Cutler, J. Guthrie and S. E. Lapi, The Use of  $^{111}\text{Ag}$  as a Tool for Studying Biological Distribution of Silver-Based Antimicrobials, *Med. Chem. Commun.*, 2013, **4**, 1015–1017.



- 14S. Chattopadhyay, K. V. Vimalnath, S. Saha, A. Korde, H. D. Sarma, S. Pal and M. K. Das, Preparation and Evaluation of a New Radiopharmaceutical for Radiosynovectomy,  $^{111}\text{Ag}$ -labelled Hydroxyapatite (HA) Particles, *Appl. Radiat. Isot.*, 2008, **66**, 334–339.
- 15N. Ukon, M. Aikawa, Y. Komori and H. Haba, Production Cross Sections of Deuteron-Induced Reactions on Natural Palladium for Ag Isotopes, *Nucl. Instrum. Methods Phys. Res. Sect. B Beam Interact. Mater. At.*, 2018, **426**, 13–17.
- 16E. W. Price and C. Orvig, Matching Chelators to Radiometals for Radiopharmaceuticals, *Chem. Soc. Rev.*, 2014, **43**, 260–290.
- 17N. C. Okoye, J. E. Baumeister, F. N. Khosroshahi, H. M. Hennkens and S. S. Jurisson, Chelators and Metal Complex Stability for Radiopharmaceutical Applications, *Radiochim. Acta*, 2019, **107**, 1087–1120.
- 18E. Boros, B. V. Marquez, O. F. Ikotun, S. E. Lapi and C. L. Ferreira, Coordination Chemistry and Ligand Design in the Development of Metal Based Radiopharmaceuticals, in *Ligand Design in Medicinal Inorganic Chemistry*, John Wiley & Sons, Ltd, 2014, pp. 47–79.
- 19D. Sneddon and B. Cornelissen, Emerging Chelators for Nuclear Imaging, *Curr. Opin. Chem. Biol.*, 2021, **63**, 152–162.
- 20T. I. Kostelnik and C. Orvig, Radioactive Main Group and Rare Earth Metals for Imaging and Therapy, *Chem. Rev.*, 2019, **119**, 902–956.
- 21C. S. Cutler, H. M. Hennkens, N. Sisay, S. Huclier-Markai and S. S. Jurisson, Radiometals for Combined Imaging and Therapy, *Chem. Rev.*, 2013, **113**, 858–883.
- 22K. S. Woodin, K. J. Heroux, C. A. Boswell, E. H. Wong, G. R. Weisman, W. Niu, S. A. Tomellini, C. J. Anderson, L. N. Zakharov and A. L. Rheingold, Kinetic Inertness and Electrochemical Behavior of Copper(II) Tetraazamacrocyclic Complexes: Possible Implications for in Vivo Stability, *Eur. J. Inorg. Chem.*, 2005, **2005**, 4829–4833.
- 23M. S. Cooper, M. T. Ma, K. Sunassee, K. P. Shaw, J. D. Williams, R. L. Paul, P. S. Donnelly and P. J. Blower, Comparison of  $^{64}\text{Cu}$ -complexing Bifunctional Chelators for Radioimmunoconjugation: Labeling Efficiency, Specific Activity, and *In Vitro/In Vivo* Stability, *Bioconjug. Chem.*, 2012, **23**, 1029–1039.
- 24L. A. Bass, M. Wang, M. J. Welch and C. J. Anderson, *In Vivo* Transchelation of Copper-64 from TETA-Octreotide to Superoxide Dismutase in Rat Liver, *Bioconjug. Chem.*, 2000, **11**, 527–532.
- 25C. F. Ramogida, E. Boros, B. O. Patrick, S. K. Zeisler, J. Kumlin, M. J. Adam, P. Schaffer and C. Orvig, Evaluation of  $\text{H}_2\text{CHXdedpa}$ ,  $\text{H}_2\text{dedpa}$ - and  $\text{H}_2\text{CHXdedpa-N,N'}$ -propyl-2-NI ligands for  $^{64}\text{Cu}(\text{II})$  Radiopharmaceuticals, *Dalton Trans.*, 2016, **45**, 13082–13090.



- 26M. Le Fur, M. Beyler, N. Le Poul, L. M. P. Lima, Y. Le Mest, R. Delgado, C. Platas-Iglesias, V. Patinec and R. Tripier, Improving the Stability and Inertness of Cu(II) and Cu(I) Complexes with Methylthiazolyl Ligands by Tuning the Macrocyclic Structure, *Dalton Trans.*, 2016, **45**, 7406–7420.
- 27S. N. Rylova, C. Stoykow, L. Del Pozzo, K. Abiraj, M. L. Tamma, Y. Kiefer, M. Fani and H. R. Mäcke, The Somatostatin Receptor 2 Antagonist <sup>64</sup>Cu-NODAGA-JR11 Outperforms <sup>64</sup>Cu-DOTA-TATE in a Mouse Xenograft Model, *PLOS ONE*, 2018, **13**, 1–16.
- 28T. J. Wadas, E. H. Wong, G. R. Weisman and C. J. Anderson, Coordinating Radiometals of Copper, Gallium, Indium, Yttrium, and Zirconium for PET and SPECT Imaging of Disease, *Chem. Rev.*, 2010, **110**, 2858–2902.
- 29S. V. Smith, Molecular Imaging with Copper-64, *J. Inorg. Biochem.*, 2004, **98**, 1874–1901.
- 30C. A. Boswell, X. Sun, W. Niu, G. R. Weisman, E. H. Wong, A. L. Rheingold and C. J. Anderson, Comparative *In Vivo* Stability of Copper-64-labeled Cross-bridged and Conventional Tetraazamacrocyclic Complexes, *J. Med. Chem.*, 2004, **47**, 1465–1474.
- 31E. H. Wong, G. R. Weisman, D. C. Hill, D. P. Reed, M. E. Rogers, J. S. Condon, M. A. Fagan, J. C. Calabrese, K.-C. Lam, I. A. Guzei and A. L. Rheingold, Synthesis of a Cross-Bridged Cyclam Derivative for Peptide Conjugation and <sup>64</sup>Cu Radiolabeling, *J. Am. Chem. Soc.*, 2000, **122**, 10561–10572.
- 32R. Ferdani, D. J. Stigers, A. L. Fiamengo, L. Wei, B. T. Y. Li, J. A. Golen, A. L. Rheingold, G. R. Weisman, E. H. Wong and C. J. Anderson, Synthesis, Cu(II) Complexation, <sup>64</sup>Cu-labeling and Biological Evaluation of Cross-bridged Cyclam Chelators with Phosphonate Pendant Arms, *Dalton Trans.*, 2012, **41**, 1938–1950.
- 33R. G. Pearson, Hard and Soft Acids and Bases, HSAB, Part 1: Fundamental Principles, *J. Chem. Educ.*, 1968, **45**, 581.
- 34A. Donzella, A. Leso, A. Arzenton, G. Bonomi, S. Bortolussi, D. Chen, S. Corradetti, M. Lunardon, E. Mariotti, E. Reniero, D. Serafini, G. S. Valli, L. Zangrando, A. Zenoni and A. Andrighetto, Monte Carlo Dosimetry of Silver-111 in Simplified Cell Geometries in the Framework of the ISOLPHARM Project, *Appl. Radiat. Isot.*, 2025, **225**, 111979.
- 35L. Morselli, A. Donzella, A. Arzenton, M. Asti, S. Bortolussi, S. Corradetti, G. D'Agostino, M. D. Luzio, M. Ferrari, A. Gandini, M. Lunardon, V. Villa, A. Salvini, L. Zangrando, A. Zenoni and A. Andrighetto, Production and Characterization of <sup>111</sup>Ag Radioisotope for Medical Use in A TRIGA Mark II Nuclear Research Reactor, *Appl. Radiat. Isot.*, 2023, **197**, 110798.
- 36K. M. El-Azony, N. M. A. Mohamed and D. A. Aloraini, Advantages and Disadvantages of Nuclear Reactions Used in Reactors or Cyclotrons, in Addition to a Theoretical Study Based on Photodisintegration on Natural Indium for <sup>111</sup>Ag Production, *Nucl. Sci. Tech.*, 2022, **33**, 14.



- 37M. Ballan, M. Tosato, M. Verona, M. Caeran, F. Borgna, E. Vettorato, S. Corradetti, L. Zangrando, M. Sgaravatto, M. Verlatto, M. Asti, G. Marzaro, F. Mastrotto, V. Di Marco, D. Maniglio, A. Bisio, A. Motta, A. Quaranta, A. Zenoni, P. Pastore, N. Realdon and A. Andrighetto, Preliminary Evaluation of the Production of Non-Carrier Added  $^{111}\text{Ag}$  as Core of a Therapeutic Radiopharmaceutical in the Framework of ISOLPHARM\_Ag Experiment, *Appl. Radiat. Isot.*, 2020, **164**, 109258.
- 38M. Tosato, M. Dalla Tiezza, N. V. May, A. A. Isse, S. Nardella, L. Orian, M. Verona, C. Vaccarin, A. Alker, H. Mäcke, P. Pastore and V. Di Marco, Copper Coordination Chemistry of Sulfur Pendant Cyclen Derivatives: An Attempt to Hinder the Reductive-Induced Demetalation in  $^{64/67}\text{Cu}$  Radiopharmaceuticals, *Inorg. Chem.*, 2021, **60**, 11530–11547.
- 39M. Tosato, M. Verona, C. Favaretto, M. Pometti, G. Zanoni, F. Scopelliti, F. P. Cammarata, L. Morselli, Z. Talip, N. P. van der Meulen, V. Di Marco and M. Asti, Chelation of Theranostic Copper Radioisotopes with S-Rich Macrocycles: From Radiolabelling of Copper-64 to In Vivo Investigation, *Molecules*, 2022, **27**, 13, 4158.
- 40M. Tosato, M. Pelosato, S. Franchi, A. A. Isse, N. V. May, G. Zanoni, F. Mancin, P. Pastore, D. Badocco, M. Asti and V. Di Marco, When Ring Makes the Difference: Coordination Properties of  $\text{Cu}^{2+}/\text{Cu}^{+}$  Complexes with Sulfur-Pendant Polyazamacrocycles for Radiopharmaceutical Applications, *New J. Chem.*, 2022, **46**, 10012–10025.
- 41M. Tosato, S. Franchi, A. A. Isse, A. Del Vecchio, G. Zanoni, A. Alker, M. Asti, T. Gyr, V. Di Marco and H. Mäcke, Is Smaller Better?  $\text{Cu}^{2+}/\text{Cu}^{+}$  Coordination Chemistry and Copper-64 Radiochemical Investigation of a 1,4,7-Triazacyclononane-Based Sulfur-Rich Chelator, *Inorg. Chem.*, 2023, **62**, 20621–20633.
- 42M. Tosato, M. Asti, M. Dalla Tiezza, L. Orian, D. Häussinger, R. Vogel, U. Köster, M. Jensen, A. Andrighetto, P. Pastore and V. Di Marco, Highly Stable Silver(I) Complexes with Cyclen-Based Ligands Bearing Sulfide Arms: A Step Toward Silver-111 Labeled Radiopharmaceuticals, *Inorg. Chem.*, 2020, **59**, 10907–10919.
- 43M. Tosato, S. Franchi, M. Dalla Tiezza, L. Orian, T. Gyr, A. Alker, G. Zanoni, P. Pastore, A. Andrighetto, U. Köster, M. Jensen, H. Mäcke, M. Asti and V. Di Marco, Tuning the Framework of Thioether-Functionalized Polyazamacrocycles: Searching for a Chelator for Theranostic Silver Radioisotopes, *Inorg. Chem.*, 2023, **62**, 20777–20790.
- 44M. Tosato, M. Asti, V. Di Marco, M. L. Jensen, J. Schell, T. T. Dang, U. Köster, M. Jensen and L. Hemmingsen, Towards In Vivo Applications of  $^{111}\text{Ag}$  Perturbed Angular Correlation of  $\gamma$ -Rays (PAC) Spectroscopy, *Appl. Radiat. Isot.*, 2022, **190**, 110508.



- 45M. Tosato, P. Randhawa, L. Lazzari, B. L. McNeil, M. Dalla Tiezza, G. Zanoni, F. Mancin, L. Orian, C. F. Ramogida and V. Di Marco, Tuning the Softness of the Pendant Arms and the Polyazamacrocyclic Backbone to Chelate the  $^{203}\text{Pb}/^{212}\text{Pb}$  Theranostic Pair, *Inorg. Chem.*, 2024, **63**, 1745–1758.
- 46M. Tosato, P. Randhawa, M. Asti, L. B. S. Hemmingsen, C. A. O'Shea, P. Thaveenrasingam, S. P. A. Sauer, S. Chen, C. Graiff, I. Menegazzo, M. Baron, V. Radchenko, C. F. Ramogida and V. Di Marco, Capturing Mercury-197m/g for Auger Electron Therapy and Cancer Theranostic with Sulfur-Containing Cyclen-Based Macrocycles, *Inorg. Chem.*, 2024, **63**, 14241–14255.
- 47M. Tosato, M. Verona, R. Doro, M. Dalla Tiezza, L. Orian, A. Andrighetto, P. Pastore, G. Marzaro and V. Di Marco, Toward Novel Sulphur-Containing Derivatives of Tetraazacyclododecane: Synthesis, Acid–Base Properties, Spectroscopic Characterization, DFT Calculations, and Cadmium(II) Complex Formation in Aqueous Solution, *New J. Chem.*, 2020, **44**, 8337–8350.
- 48M. Trose, M. Dell'Acqua, T. Pedrazzini, V. Pirovano, E. Gallo, E. Rossi, A. Caselli and G. Abbiati, [Silver(I)(Pyridine-Containing Ligand)] Complexes As Unusual Catalysts for A3-Coupling Reactions, *J. Org. Chem.*, 2014, **79**, 7311–7320.
- 49H. Tsukube, S. Shinoda, J. Uenishi, T. Hiraoka, T. Imakoga and O. Yonemitsu, Ag<sup>+</sup>-Specific Pyridine Podands: Effects of Ligand Geometry and Stereochemically Controlled Substitution on Cation Complexation and Transport Functions, *J. Org. Chem.*, 1998, **63**, 3884–3894.
- 50S. El Ghachtouli, C. Cadiou, I. Déchamps-Olivier, F. Chuburu, M. Aplincourt and T. Roisnel, (Cyclen- and cyclam-pyridine)copper Complexes: The Role of the Pyridine Moiety in Cu<sup>II</sup> and Cu<sup>I</sup> Stabilisation, *Eur. J. Inorg. Chem.*, 2006, **2006**, 3472–3481.
- 51N. Bernier, J. Costa, R. Delgado, V. Félix, G. Royal and R. Tripier, Monopicolinate Cyclen and Cyclam Derivatives for Stable Copper(II) Complexation, *Dalton Trans.*, 2011, **40**, 4514–4526.
- 52A. Bianchi, M. Micheloni and P. Paoletti, Thermodynamic Aspects of the Polyazacycloalkane Complexes with Cations and Anions, *Coord. Chem. Rev.*, 1991, **110**, 17–113.
- 53E. Boros, P. Comba, J. W. Engle, C. Harriswangler, S. E. Lapi, J. S. Lewis, S. Mastroianni, L. M. Mirica, C. Platas-Iglesias, C. F. Ramogida, R. Tripier and M. Tosato, Chemical Tools to Characterize the Coordination Chemistry of Radionuclides for Radiopharmaceutical Applications, *Chem. Rev.*, 2025, **125**, 12030–12068.
- 54T. A. Kaden, Model Complexes for Biologically Active Copper, *Portugaliae Electrochimica Acta*, 1993, **10**, 109-120.
- 55M. Tosato, M. Boniburini, F. Faglioni, F. Genua, M. Mari, J. Storchi, S. Franchi, M. Asti and E. Ferrari, Thwarting Isomerization through Rigidity: A Promising HBED Derivative for the Chelation of Gallium-68, *Inorg. Chem.*, 2025, **64**, 18673–18686.
- 56V. Di Marco, PhD Thesis, University of Padova, 1998.



- 57 <http://www.hyperquad.co.uk/> (accessed April 20 2026).
- 58 C. F. J. Baes and R. E. Mesmer, *The Hydrolysis of Cations*, Wiley-Interscience, New York, 1976.
- 59 A. Rockenbauer and L. Korecz, Automatic Computer Simulations of ESR Spectra, *Appl. Magn. Reson.*, 1996, **10**, 29–43.
- 60 Gaussian 16, Revision B.01, Frisch, M.J., Trucks, G.W., Schlegel, H.B., Scuseria, G.E., Robb, M.A., Cheeseman, J.R.; Scalmani, G.; Barone, V.; Petersson, G.A.; Nakatsuji, H.; Li, X.; Caricato, M.; Marenich, A.V.; Bloino, J., Janesko, B.G., Gomperts, R., Mennucci, B., Hratchian, H.P., Ortiz, J.V., Izmaylov, A.F., Sonnenberg, J.L., Williams-Young, D., Ding, F., Lipparini, F., Egidi, F., Goings, J., Peng, B., Petrone, A., Henderson, T., Ranasinghe, D., Zakrzewski, V.G., Gao, J., Rega, N., Zheng, G., Liang, W., Hada, M., Ehara, M., Toyota, K., Fukuda, R., Hasegawa, J., Ishida, M., Nakajima, T., Honda, Y., Kitao, O., Nakai, H., Vreven, T., Throssell, K., Montgomery Jr., J.A., Peralta, J.E., Ogliaro, F., Bearpark, M.J., Heyd, J.J., Brothers, E.N., Kudin, K.N., Staroverov, V.N., Keith, T.A., Kobayashi, R., Normand, J., Raghavachari, K., Rendell, A.P., Burant, J.C., Iyengar, S.S., Tomasi, J., Cossi, M., Millam, J.M., Klene, M., Adamo, C., Cammi, R., Ochterski, J.W., Martin, R.L., Morokuma, K., Farkas, O., Foresman, J.B., Fox, D.J. Gaussian, Inc., Wallingford CT (2016) GaussView 5.0. Wallingford, E.U.A.
- 61 A. D. Becke, Density-functional Thermochemistry. III. The Role of Exact Exchange, *J. Chem. Phys.*, 1993, **98**, 5648–5652.
- 62 P. J. Hay and W. R. Wadt, Ab Initio Effective Core Potentials for Molecular Calculations. Potentials for K to Au Including the Outermost Core Orbitals, *J. Chem. Phys.*, 1985, **82**, 299–310.
- 63 E. Cancès, B. Mennucci and J. Tomasi, A New Integral Equation Formalism for the Polarizable Continuum Model: Theoretical Background and Applications to Isotropic and Anisotropic Dielectrics, *J. Chem. Phys.*, 1997, **107**, 3032–3041.
- 64 B. Mennucci and J. Tomasi, Continuum Solvation Models: A New Approach to the Problem of Solute's Charge Distribution and Cavity Boundaries, *J. Chem. Phys.*, 1997, **106**, 5151–5158.
- 65 S. F. Boys and F. Bernardi, The Calculation of Small Molecular Interactions by the Differences of Separate Total Energies. Some Procedures with Reduced Errors, *Mol. Phys.*, 1970, **19**, 553–566.
- 66 H. Yang, F. Gao, B. McNeil, C. Zhang, Z. Yuan, S. Zeisler, J. Kumlin, J. Zeisler, F. Bénard, C. Ramogida and P. Schaffer, Synthesis of DOTA-pyridine Chelates for <sup>64</sup>Cu Coordination and Radiolabeling of αMSH Peptide, *EJNMMI Radiopharm. Chem.*, 2021, **6**, 3.



## Data Availability Statement

View Article Online  
DOI: 10.1039/D6QI00525J

The authors confirm that the data supporting the findings of this study are available within the article and its supplementary information (SI).

